Journal of Materials Chemistry A

ROYAL SOCIETY OF CHEMISTRY

PERSPECTIVE

View Article Online
View Journal | View Issue

Cite this: J. Mater. Chem. A, 2022, 10, 5899

CO_2 electrochemical reduction on metal–organic framework catalysts: current status and future directions

Denise Narváez-Celada and Ana Sofia Varela *

Metal–Organic Frameworks (MOFs) are modular materials made from inorganic metal ions or clusters bonded through organic linkers to form an ordered, porous network. The high surface area and the tailorable nature of MOFs make them ideal candidates for catalyst design. Therefore, they have been investigated as catalysts for a variety of processes including electrochemical reactions. Herein, we focus on their use as catalysts for the electrochemical CO_2 reduction reaction (CO2RR), which is a promising technology for converting waste CO_2 into valuable carbon-based chemicals. Recent studies have shown that CO_2 can be selectively reduced using MOF-based catalysts, furthermore, MOFs in catalysis have the key advantage of using well-defined single-atom active sites. This is helpful to understand and optimize the structural parameters that control their performance towards the CO2RR. Despite these advantages and the promising early results, there are some important limitations that need to be overcome, namely the poor conductivity and stability of MOFs, which need to be addressed in future studies. In addition, more systematic studies are needed to gain fundamental understanding of the structural parameters that control the performance of MOF-based catalysts.

Received 6th December 2021
Accepted 12th January 2022

DOI: 10.1039/d1ta10440c

rsc.li/materials-a

1. Introduction

a. CO_2 electrochemical reduction

In order to mitigate the effects of CO_2 on global climate, it will be necessary to eliminate the emissions of this greenhouse gas.[1] To achieve this ambitious goal, a combination of efforts will be needed to replace fossil fuels, when possible, and to develop new CO_2 capture, storage and utilization (CCUs) technologies.[2] The CO_2 electrochemical reduction reaction (CO2RR) represents a promising utilization technology to convert waste CO_2 streams into useful chemicals. Contrary to other chemical processes, the CO2RR has the advantage of taking place under ambient conditions and that the hydrogen needed to reduce

Instituto de Química, Universidad Nacional Autónoma de México, Ciudad Universitaria, Circuito exterior s/n, Del. Coyoacán, 04510, Mexico. E-mail: asvarela@iquimica.unam.mx

Denise Narváez-Celada obtained her BSc in Chemistry at the National Autonomous University of Mexico (UNAM), where she earned the Gabino Barreda award for achieving the highest GPA in her class. After working in industry for 3 years, she is currently pursuing her graduate studies in Dr Varela's group, focusing on the development of MOF-based electrodes for electrocatalytic CO_2 reduction.

Ana Sofia Varela studied Chemistry at the National Autonomous University of Mexico (UNAM) and obtained her masters at the Autonomous University of Madrid. She received her PhD from the Technical University of Denmark with the thesis "The catalysis of CO_2 electroreduction and related processes". After completing a postdoc at TU Berlin with Prof Strasser, she started her research group on electrocatalysis at UNAM, focusing on new materials as electrocatalysts for CO_2 reduction. In recognition of her work, she has received different recognitions including the "International Rising Talents" on behalf of L'Oreal-UNESCO in 2019.

CO_2 comes from water. Furthermore, energy is supplied as electricity, which can easily be generated from renewable sources, making it a carbon neutral process.[3]

One of the key challenges to ensure an efficient CO2RR is the selectivity of the process. In aqueous electrolytes, the reaction is in competition with the hydrogen evolution reaction (HER, reaction (1)), which occurs at low overpotential on several catalysts:

$$2H^+ + 2e^- \rightarrow H_2 \quad E_0 = 0 \text{ V } \textit{vs.} \text{ RHE} \quad (1)$$

In addition, there are several carbon-based products that can be formed during CO_2 reduction. The most common are those requiring only two electron transfers, namely formic acid[4] and CO according to the following reactions:[5]

$$CO_2 + 2H^+ + 2e^- \rightarrow HCOOH \quad E_0 = -0.22 \text{ V } \textit{vs.} \text{ RHE} \quad (2)$$

$$CO_2 + 2H^+ + 2e^- \rightarrow CO + H_2O \quad E_0 = -0.11 \text{ V } \textit{vs.} \text{ RHE} \quad (3)$$

CO is an interesting product as it is employed as a precursor in several industrial processes, such as methanol production and the hydroformylation of olefins. Moreover, if a mixture of CO and H_2 is produced in an electrochemical cell, it can be directly used as syngas and transformed into other valuable chemicals *via* the Fischer–Tropsch process.

As seen in Fig. 1, a key difference in the mechanism for CO *vs.* formate production is the bond formed between CO_2 and the catalyst.[6] In general, it has been observed that catalysts that bind CO_2 through oxygen form HCOOH as a major product, while the binding *via* carbon results in CO formation.[7] In this case, the rate-limiting step is usually the first electron transfer, which has been proposed as a coupled proton/electron transfer or a decoupled proton/electron transfer. The main difference between these two proposed mechanisms is their pH dependency, in the first case the CO production rate is affected by proton concentration, while the second mechanism will be independent of pH.[8] Once CO is formed, it can be desorbed from the surface as a reaction product or it can be further reduced to form hydrocarbons and alcohols according to the following reactions:

$$CO_2 + 8H^+ + 8e^- \rightarrow CH_4 + 2H_2O \quad E_0 = 0.17 \text{ V } \textit{vs.} \text{ RHE} \quad (4)$$

$$2CO_2 + 12H^+ + 12e^- \rightarrow C_2H_4 + 4H_2O \quad E_0 = 0.08 \text{ V } \textit{vs.} \text{ RHE} \quad (5)$$

$$2CO_2 + 12H^+ + 12e^- \rightarrow C_2H_5OH + 3H_2O \quad E_0 = 0.08 \text{ V } \textit{vs.} \text{ RHE} \quad (6)$$

Fig. 1 shows the two proposed mechanisms for CO reduction.[9,10] In the first pathway, CO is reduced and protonated to form the key intermediate *CHO, which then is reduced into methane and multi-carbon products such as ethylene.[11,12] The second pathway involves the coupling of two *CO molecules or of *CO and *CHO as a rate limiting step, to form multi-carbon products.[13] This last mechanism is also independent of pH and tends to be the dominant one at low overpotentials.[14]

The direct reduction of CO_2 into these multi-carbon products is highly desired given their high energy content and relevance in the chemical industry. Nevertheless, it is challenging to obtain such products, so they are generally reported only as minor products. Copper heterogeneous catalysts are a remarkable exception, yet their selectivity is still too low and the energy requirements too high for technological applications.[15,16]

b. Electrocatalysts for CO_2 electrochemical reduction

The distribution of products, as well as the energy efficiency and stability of the electrochemical process, are highly dependent on the catalyst material. Therefore, many efforts have been dedicated to the development of novel, cost-efficient catalysts to reduce CO_2 selectively into a specific product at low overpotentials and with long-term stability. Copper's unique ability to produce hydrocarbons makes it one of the most studied materials as an electrocatalyst for the CO2RR.[16,17] Other metal catalysts such as Au and Ag[5] have been widely studied as catalysts for CO production, while Sn catalysts have been used for formate production.[7] Another common approach is the use of homogeneous catalysts based on metal complexes, such as metal porphyrins and phthalocyanines,[18] which have been reported as highly selective towards CO production, yet they tend to have solubility issues, especially in aqueous electrolytes, and they are not recovered easily. While initial studies focused on either metal-based heterogeneous catalysts[19] or molecular catalysts,[20,21] in recent years there has been a growing interest in the development of heterogeneous catalysts made of abundant elements, containing highly active sites resembling those on molecular catalysts. In this context, single-atom catalysts which, as their name suggests, are made up of isolated active centers, have emerged as a promising alternative.[22,23] A common example of these single-atom catalysts are metal-doped carbon materials, in which the metals are incorporated into a carbon support *via* coordination with a heteroatom, commonly N, to form metal and nitrogen doped carbon materials (MNCs).[24] These materials are generally prepared using heat treatment to incorporate nitrogen and metal atoms into a carbon substrate. This process results in inhomogeneous materials containing a variety of chemical functionalities, including metal centers coordinated to nitrogen in MN_x moieties, similar to those on metal macrocycles.[25]

Several studies have shown that MNC materials have a remarkable catalytic performance, especially for CO production, reaching CO partial current densities of several hundred mA cm^{-1}.[26] Despite these promising results, the inhomogeneity of MNC materials makes it challenging to identify the contribution of the different metal and nitrogen moieties to the catalytic activity.[27] Therefore, it is necessary to study better defined heterogeneous catalysts to establish structure–activity correlations, which is crucial knowledge for the design of novel catalysts.

As we will discuss throughout this work, metal–organic frameworks (MOFs) can be used as well-defined single-atom catalysts towards the electrochemical CO2RR. While the versatile nature of these materials presents an opportunity to

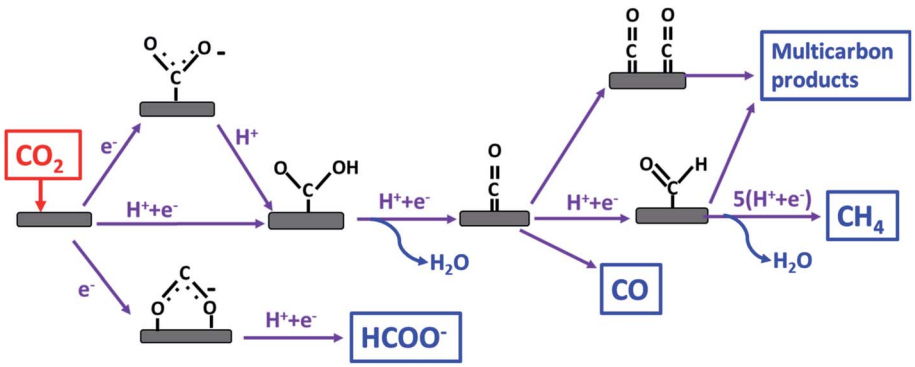

Fig. 1 Scheme of the CO_2 reduction pathway toward different reaction products.

establish structure–activity correlations and to optimize the active site, there are still important challenges to overcome in order to ensure a good electrocatalytic performance of MOFs towards the CO2RR.

2. MOFs as electrocatalysts

Metal–organic frameworks (MOFs) are porous, crystalline materials constructed from a diversity of organic linkers and inorganic building blocks, which results in extremely versatile materials (Fig. 2a). This tailorable nature and their structural diversity make them ideal candidates for catalyst optimization. In addition, the porosity of MOFs facilitates the transport of reactants to the active sites, reducing mass transport limitations, while their large surface area results in a high number of well-defined active sites that can participate in the catalytic process.[28–30]

The metal active sites in MOFs can be those present in the inorganic nodes, or they can be incorporated into the structure of a pristine MOF, usually *via* post-synthetic modifications, to metalate the organic linkers containing donor atoms such as N, O or S. These metal species are homogeneously dispersed throughout the material; and their chemical environment, in terms of coordination and oxidation number, is well defined, facilitating an in-depth understanding of how the nature of the active sites affects its catalytic properties. Also, the chemical environment of the active sites can be further modified by choosing different building blocks, which can be used to tune their catalytic properties by changing the metal center, its coordination, and the electronic properties of the linker. In addition, changing the size of the linker also allows the modification of the shape and size of the channels and pores of the material, to gain insight into transport phenomena.

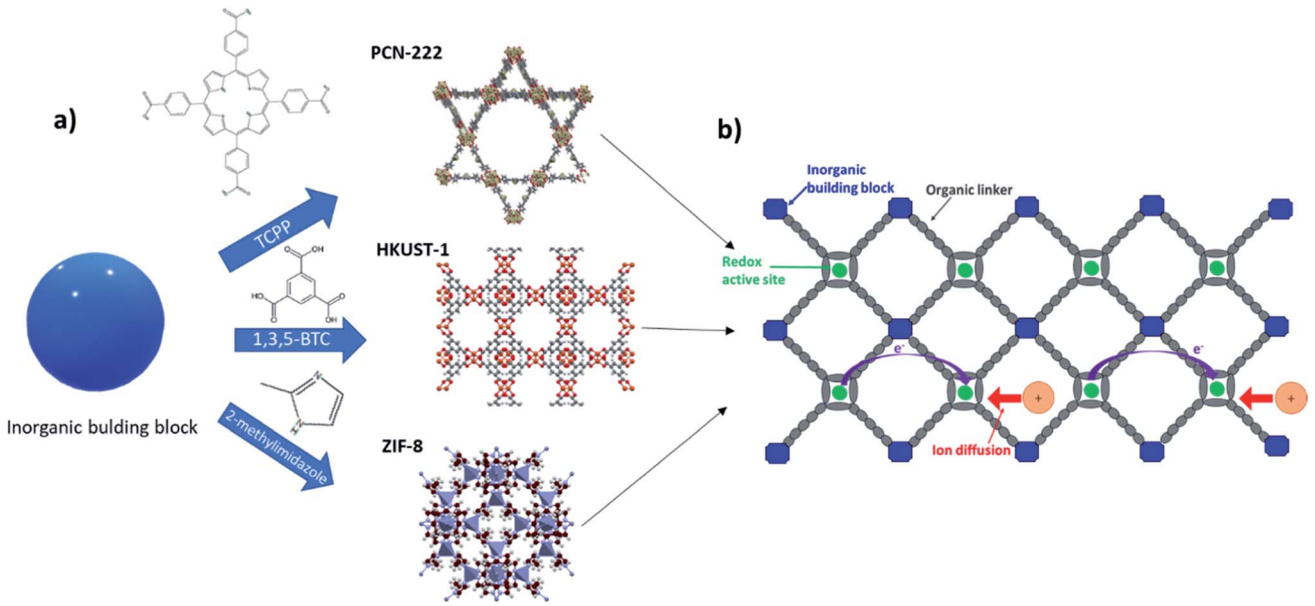

Fig. 2 (a) Diagram showing different MOFs families depending on the nature of the linker. MOF structures adapted from ref. 31–33. (b) Scheme of the redox hopping mechanism through the internal MOF structure.

MOFs have been used for a variety of catalytic and electrocatalytic processes such as oxygen reduction and evolution reactions and the CO2RR,[34–39] showing encouraging performance for their application in electrochemistry. Despite these promising early results, there are some important limitations when using MOFs for electrochemical applications to be addressed, mainly their poor stability and electrical conductivity.

a. Electrical conduction in MOFs

An efficient charge transport in MOF-based electrodes is crucial for their application in electrocatalysis. Poor electrical conductivity reduces the number of available active sites, and the reaction would only occur at the metal centers in direct proximity to the electrode, which would limit the maximum possible catalytic current. An approach to improve the conductivity of MOFs is the use of composites made of a mixture of the MOF and certain conductive materials, such as carbon. This strategy has been proven to be effective to enhance the performance of MOF-based electrodes.[40] Despite the improvements observed with the use of composites, having a highly conductive MOF is essential to ensure a good electric response.

Charge transport in MOFs is fundamentally different from that observed in traditional electrodes made of metals, conductive carbon, or metal oxides. While for some MOFs the delocalized charge allows band transport, for the vast majority of them, the charge transfer occurs *via* an electron hopping mechanism, in which the charge carriers (electrons or holes) move in between neighboring redox centers.[41,42] As seen in Fig. 2b, this process is accompanied by counter-ion diffusion through the MOF structure to maintain electroneutrality. Therefore, the charge transfer in MOFs can be studied as a diffusion phenomenon and the diffusion coefficient (D_{app}), obtained *via* Cotrell analysis, together with the hopping distance (r), can be used to estimate the electron exchange rate constant (k)[43] *via* the following equation:

$$k_{hopping} = \frac{D_{hopping}}{r^2} \quad (7)$$

The experimentally observed diffusion coefficient involves both the diffusion coefficients of electrons from one redox center to another (D_e) and the ion diffusion through the MOF structure (D_i).[44] D_e is dependent on the total redox active linker concentration C_p^0 and on the electron transfer rate k_e, which assumes homogeneous self-exchange reactions with the nearest neighbours ($k_e = 6k_{ex}$),[42] according to:

$$D_e = \frac{k_e}{6} C_p^0 r^2 \quad (8)$$

Consistently, experimental observations have shown that the charge transfer rate in MOFs is affected by the metal center, increasing with the self-exchange rates of its redox process.[44,45]

The counterion diffusion is also influenced by the size and concentration of the ions in solution, the MOF's pore size and its ion pairing ability. As a result, the choice of electrolyte can have a significant effect on the electrochemical response of MOF-based electrodes. For instance, Celis-Salazar *et al.* found that ion diffusion on a family of metallocene-doped MOFs was faster when tetrakis(pentafluorophenyl)borate ($TFAB^-$) was used as counterion in comparison with the results obtained using hexafluorophosphate (PF_6^-), which was attributed to a lower ion-pairing association in the first case, facilitating the diffusion through the MOF's network.[44] Finally, the ratio between the size of the counterion and the MOF channels should also be considered in the optimization of charge transport. Bulkier ions will diffuse slower through the MOF, especially if it is made of narrow channels. Consistently, in the study by Meng *et al.* it was observed that modification of the pore size is a promising alternative to tune charge transfer in MOFs. Since ion diffusion limits the overall charge transfer rate, increasing the pore size results in a larger transfer rate constant, k_{hop}.[46] However, a large pore size could also have a negative impact, as a large hopping distance would limit electron diffusion.

This illustrates the complexity of charge transport in MOFs *via* redox hopping, which remains a major challenge for the applications of MOFs in electrocatalysis. Therefore, different strategies have been used to enhance MOF conductivity. One common strategy is the post-synthetic introduction of guest redox molecules into the frameworks.[47,48] These guest molecules form charge transport pathways through guest to guest or guest to framework interactions. Unfortunately, this strategy can result in the blocking of pore channels and a drop in surface area, which are key properties for electrocatalysis. Thus, it is important to carefully choose the MOF and guest to minimize these effects. An interesting example is the work by Kung *et al.*, who improved the conductivity of NU-1000 by selectively loading nickel bis(dicarbollide) in the micropores of the MOF while leaving the mesopores unoccupied.[49] Recently, this strategy was used to improve the electrocatalytic activity of MOF-545-Co for the CO2RR by the introduction of cobaltocene as a potential donor and carrier to enhance the electron density within the MOF structure. The presence of this guest molecule improved the catalytic performance of the system, going from an initial maximum F.E. towards CO formation of 55% at −0.8 V *vs.* RHE to a F.E. of 97% at −0.7 V, showing that the MOF's conductivity has a crucial role on its efficiency as an electrocatalyst.[50]

A more attractive alternative to overcome charge transport limitations is the development of conductive MOFs with band charge transport. This can be achieved by having charge delocalization within the MOF. In this regard, linkers containing sulfur or nitrogen coordinating to the metal centers can improve energy matching and metal–ligand orbital overlap and facilitate charge transport.[48] For instance, in the work of Sun *et al.*, the linker 2,5-disulfhydrylbenzene-1,4-dicarboxylic acid is used to form Mn–S conduction chains with high charge mobility.[51] Another approach is to have π-conjugation, to allow the long-range movement of charge carriers through the MOF, which has proven to be an effective strategy to design 2D conductive MOFs.[52–54] The presence of π electrons also promotes the conduction of electrons *via* π-stacked pathways, as observed in the works from Xie *et al.*[55] and Park *et al.*[56] While this strategy has resulted in highly conductive MOFs, π-stacking

of the organic linkers might result in interpenetration or a non-porous structure, reducing the available surface area for electrocatalysis.

A particularly interesting class of 2D conductive MOFs are the metal–organic Kagome lattices or metal–organic graphene analogues (MOGs). These materials consist of square-planar metal ions and aromatic organic linkers which, as their name indicates, assemble into Kagome lattice patterns, which makes them structural analogs to graphene.[57] A prototypical example of this kind of conductive MOFs is $Ni_3(HITP)_2$·(HITP = 2,3,6,7,10,11-hexaiminotriphenylene). This MOG has remarkable electrical properties due to full in-plane charge delocalization, which leads to a high conductivity value in the bulk and film form: 2 and 40 S cm^{-1}, respectively.[52] Furthermore, the conductivity of this species has an interesting behavior: in its bulk form it acts as a metal conductor, but it has semiconductor properties when it is exfoliated into thin films. Its conductivity is also observed to increase with temperature, which is consistent with a non-zero band gap value, yet this increase is not exponential like it would be expected for a semiconductor.[58] Additionally, theoretical[57] and experimental[59] studies have shown that the electronic properties of this system are highly tunable by means of metal substitution, alloying and morphology modification. The synthesis of binary alloys of this MOG, $(M_xM'_{3-x})(HITP)_2$ (MM′= CuNi, CoNi, CoCu), has enabled a variation of electrical conductivity in this material of over 4 orders of magnitude.[59]

The outstanding properties of this class of conductive MOFs make them promising options to be tested for electrocatalytic applications, yet there are only a few studies showing their potential in this area. For instance, the aforementioned $Ni_3(HITP)_2$ was used as an efficient ORR catalyst,[60] while the $Co_3(HITP)_2$ MOG showed very high electrocatalytic activity towards OER, comparable to commercial RuO_2 and IrO_2 catalysts.[61] Likewise, a related 2D conductive MOF with a Kagome lattice structure, $Ni_3(Ni_3 \cdot HAHATN)_2$, exhibited a low onset potential and good stability as an electrocatalyst towards the hydrogen evolution reaction.[62]

In the case of CO2RR, conductive phthalocyanine-based MOFs have been tested in works by Yi *et al.*[63] and Meng *et al.*[64] As we will discuss in Section 4, these two studies reported higher catalytic currents in comparison with other MOF-based electrocatalysts and high faradaic efficiencies towards selective CO formation, showing the potential of this family of conductive MOFs as efficient CO2RR electrocatalysts.

Despite these early encouraging results of conductive MOFs in electrocatalysis, the number of conductive MOFs reported so far is still limited, reducing the opportunities for catalyst optimization. Therefore, the development of more conductive MOFs with new ligands and new topologies is needed to establish structure–activity correlations which will be needed for catalytic optimization.

b. Stability of MOF-based electrodes

The application of MOFs in electrocatalysis is also contingent on developing MOF-based electrodes that are stable under long periods of electrochemical testing. In this regard, two critical points should be considered when evaluating the stability of MOFs for electrochemical applications: (1) the attachment of the MOF to the electrode surface (2) structural stability in the electrochemical medium and under reducing or oxidizing conditions.

As we will discuss in the later sections, the long-term stability of a MOF on the electrode surface is impacted by the preparation method. In addition to the chemical stability of the catalyst material, it is important to ensure a strong adhesion to the electrode surface to assure that the catalytic process does not take place on the bare electrode. In general, chemical attachment to the surface results in a stronger and more stable film adhesion in comparison with physical attachment. Therefore, the direct growth of MOFs forming chemical bonds with the electrode surface is an attractive strategy to prepare long-lasting films.

A good attachment to the electrode, however, does not correlate with the chemical stability of the MOF under reaction conditions. The integrity of the MOF might be affected by interactions with the electrolyte, reaction intermediates or applied current, resulting in dissolution of the MOF, collapse of the framework or formation of MOF-derived oxides. In particular, the metal–ligand bond is a weak point of the structure that is susceptible to chemical reactions such as hydrolysis.[65] Therefore, the chemical stability of a MOF is strongly affected by the properties of both the linker and the inorganic cluster.[66] For instance, a higher pKa of the coordination site of the linkers will result in a stronger bond with the metal centers, which are Lewis acids, while hydrophobic ligands can be used to protect the metal center.[67]

High valence metals coordinated with oxygen donor ligands tend to form strong coordination bonds, resulting in MOFs with good chemical stability, as is the case for MOFs containing metal ions such as Zr^{4+} or Ti^{4+} and ligands with carboxylate groups. Despite the stability in aqueous media of several of these MOFs made of high valence metals, they tend to be unstable at certain pH values.[36] In general, MOFs built from low-valent metal and azolate ligands can be easily hydrolyzed in acidic conditions, while MOFs containing high-valent metal ions and carboxylate ligands tend to decompose in alkaline media. In addition to the pH, the presence of certain ions in solution can be destructive for MOFs, since anions such as phosphate, carbonate or fluoride can act as competing species to the carboxylic ligands and coordinate with the metal centers.[68] This can be particularly problematic during the CO2RR, since this process is usually carried out under aqueous neutral electrolytes, typically CO_2 saturated bicarbonate or phosphate buffer, which can contribute to MOF instability.

Therefore, non-aqueous electrolytes, such as tetrabutylammonium hexafluorophosphate ($TBAPF_6$) in acetonitrile or DMF, have been used to study the catalytic activity of MOFs that are unstable in aqueous electrolytes. Using these organic solvents has the advantage of a high CO_2 solubility, which can reduce mass transport limitations. In addition, their proton concentration is low, inhibiting the competing process of the hydrogen evolution reaction.[69] Nevertheless, aqueous electrolytes are highly desired, as water is a safe and abundant solvent that can be used in large scale processes.[70] For this reason, the use of catalytically active MOFs stable in the presence of

bicarbonate ions is necessary for future applications. MOFs made of anionic and nitrogen-containing linkers such as ZIFs are usually highly stable in water in a wide pH range,[71] consistently, this family of MOFs has been successfully tested as catalysts towards the CO2RR in aqueous electrolytes.[72–75]

A final stability issue to be addressed, is that the flow of electrons through the material can also contribute to the instability of MOF-based electrodes. On one hand, charging of the MOF can induce delamination of the films, reducing the number of active sites attached to the electrode; while the redox process occurring on the MOF's linkers or inorganic nodes might be irreversible, resulting in MOF degradation. Therefore, it is important to take into consideration the redox chemistry of the individual MOF's building blocks, and work with components that have reversible redox processes or are inert under the working potential window.[76]

All these factors can contribute to structural evolution of the MOF during the catalytic process, which might lead to deactivation of the MOF, loss of surface area or the formation of an active phase different to that of the starting material. For instance, Huang *et al.* observed the structural evolution of a 3D pillar-layered MOF, attributed to the oxidative conditions during OER. In particular, the authors proposed that the pillars are selectively oxidized and removed, leaving the 2D layers intact.[77] In another study, Rui *et al.* observed the formation of NiO nanograins after OER on 2D Ni-MOF nanosheets decorated with Fe-MOF nanoparticles.[78] Similarly, Yang *et al.* reported the formation of Cu nanoparticles after CO_2 electrolysis on a Cu–adenine MOF. These results suggested the studied MOF was not responsible for the remarkable formation of methane and ethylene and that the active phase was in fact the Cu nanoparticles, known to be selective towards hydrocarbon formation.[79] These examples highlight the importance of material characterization, before and after the electrocatalytic process, to identify the active species and to understand the structural evolution of MOFs under catalytic conditions. While post-electrolysis characterization, such as TEM, can reveal relevant information, *operando* techniques will be crucial to identify active species, since they might only be stable under reaction conditions. For instance, Zhao *et al.* observed a potential-induced two-step reconstruction at the metal nodes inside a NiCo-MOF-74 during OER. At the working potential, the formation of $Ni_{0.5}Co_{0.5}OOH_{0.75}$ was proposed as the catalytic species. The pristine MOF, however, was recovered after reaction. Thus, the active species could only be detected under the OER conditions.[80] To our knowledge, such dynamic behavior has not yet been observed during CO2RR, but it should not be discarded. Future studies focusing on the structural evolutions of MOFs under CO2RR conditions will be key to establish structure–activity correlations and to understand the different effects that contribute to the stability of MOF-based catalysts.

3. Preparation of MOF-based electrodes

As discussed in the previous section, the preparation method plays an important role in the attachment of the catalyst material to the electrode's conductive substrate. Furthermore, it impacts the morphology and thickness of the catalyst film and thus could affect the catalytic activity of the MOF-based electrode and its long-term stability.

The preparation of MOF-based electrodes does not vary widely across applications. The basic process consists of dispersing the MOF over a conductive substrate, which can be achieved *via* physical interactions or through the formation of chemical bonds between the substrate and the MOF. Despite the diversity of synthetic approaches used for MOF preparation, some of them, like direct growth over metal foils or foams, have not yet been thoroughly explored in the preparation of CO2RR catalysts. By contrast, for other electrochemical reactions of interest, such as OER and ORR, these methods have shown to be promising synthetic routes to overcome some of the challenges regarding poor stability of MOF-based electrodes.[81]

a. Drop casting

The most common method used to prepare MOF-based electrodes is the preparation of catalyst suspensions, commonly known as inks, followed by drop casting over diverse substrates, as illustrated in Fig. 3a. The preparation of catalyst inks is a very versatile and straightforward process, with a wide variety of solvents used as dispersion media. The powder catalyst is suspended in a solvent or solvent mixture of choice, together with a binding agent; Nafion® being the most common. Other binders should also be explored, in order to find other options that may be more appropriate for working in neutral or alkaline electrolytes. Suitable conductive materials, like carbon black,[72] can be mixed into the catalyst ink to increase the material's electrical conductivity, which, as we mentioned in Section 2, is a strategy to overcome the drawback of MOFs' low electrical conductivity.

The resulting solution is then drop casted or dip-coated onto the chosen substrate and dried so that an apparently uniform film is formed. Different materials can be used to deposit the ink on, but it is important that the electrode is made of a conductive material. Common working electrode substrates include GC (glassy carbon), FTO (fluorine-doped tin oxide), and carbon paper.[38,72,82]

While drop casting is certainly a facile and versatile method to prepare MOF-based electrodes, it is difficult to control the thickness and morphology of the resulting MOF films. Additionally, charge transfer between the electrode surface and the MOF may be inefficient and contribute to the low conductivity of the MOF-based electrode. Furthermore, as shown in the work of Jiang *et al.*, who observed deactivation of their Cu-NPC-4 MOF detected by the loss of crystallinity through PXRD after various electrocatalytic cycles for ORR,[83] MOF based films prepared by drop casting suffer from poor stability, limiting their ability to serve as electrodes for long reaction times or repeated cycles.

The catalyst ink can also be used to prepare gas diffusion electrodes (GDEs) by airbrushing the solution on a piece of porous carbon paper. GDEs have the advantage of reducing mass transport limitations, caused by the low solubility of CO_2 in the electrolyte, by feeding the CO_2 gas on one side of the

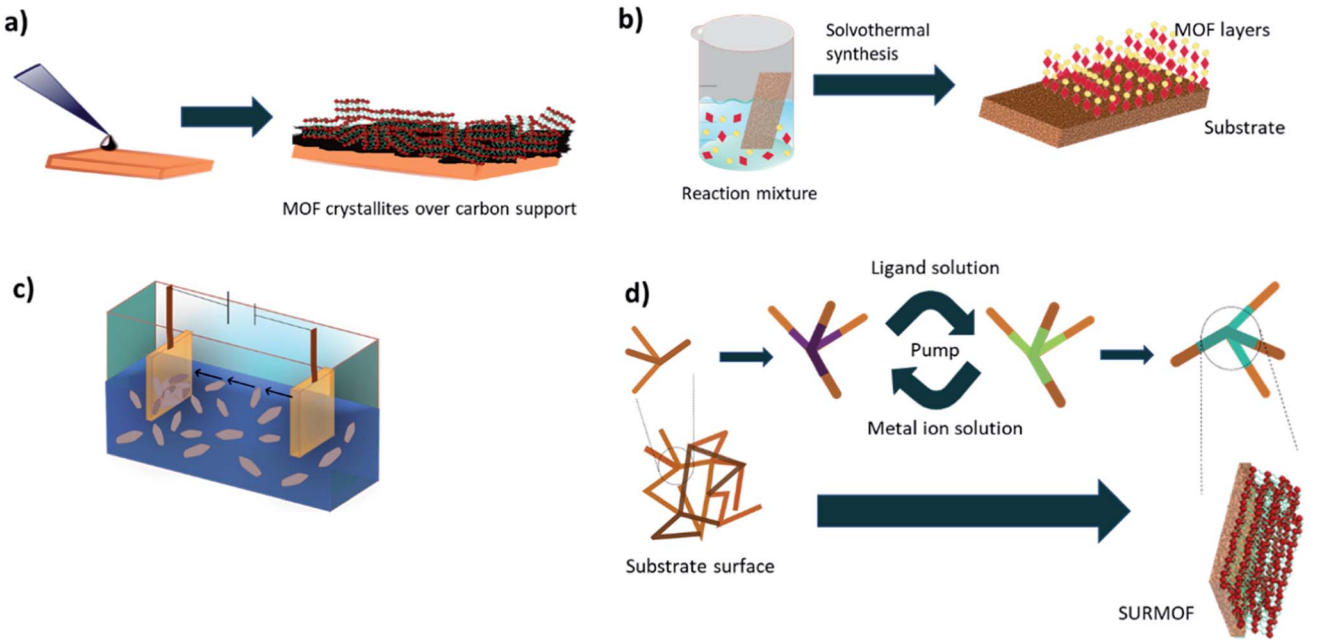

Fig. 3 Depiction of different MOF-based electrode construction methods: (a) drop casting, (b) direct growth, (c) electrochemical synthesis, (d) liquid phase epitaxy (LPE).

electrode. This approach was tested by Albo and Perfecto-Irigaray's groups for HKUST-1 type Cu MOFs. Despite some promising results in terms of their high selectivity towards hydrocarbon formation, these MOF-based GDEs were not stable during long-term CO_2 electrolysis, indicating that there is also room for optimization of the inks used for this type of electrode construction.[84,85]

It is necessary to keep in mind that while polymeric binders such as Nafion can be beneficial for the attachment of the catalyst material to the electrode surface, they also increase its resistance, limit mass transfer and can block some of the MOFs' active sites, leading to a decrease of the desired catalytic activity.[86] For these reasons, other methods have been developed to prepare stable and well-defined MOF-based electrodes.

b. Direct growth

Alternatively, the direct growth of MOF films onto conductive substrates is an attractive option that presents many key advantages: (i) the MOF is strongly attached to the substrate *via* chemical bonding, enhancing stability and charge transfer. (ii) The thickness of the resulting film can be controlled, to optimize charge transfer and catalyst utilization.[81]

The simplest approach to direct growth of MOF films is the solvothermal synthesis of the material with a piece of substrate immersed in the reaction mixture, as shown in Fig. 3b. The most common substrates used for this approach are metal foams, FTO glass and glassy carbon. For this technique to work, it is necessary to have a nucleation point where the MOF growth can begin. Based on some observations,[87] an analogy of direct MOF growth can be done with the Volmer–Weber mode; where an initial nucleation takes place, followed by the growth of pre-formed crystals and secondary nucleation, where gaps near the pre-formed crystals are filled by post-formed crystal growth. To facilitate the direct growth on carbon electrodes, these are usually modified to incorporate functional groups such as carboxylic groups on their surface, which can form coordination bonds with the building units of the MOF. In FTO substrates, the metal oxides on the surface function as homogeneous nucleation sites, where the nucleation precursors anchor until a sufficient amount of them is formed and nanocrystal seeds start to assemble on the surface.[88] Therefore, FTO is a common substrate for this kind of MOF-based electrodes, despite its low conductivity when compared with carbon.

The direct growth strategy can be aided by other techniques that involve the modification of the substrate prior to the synthesis, to have better control of the growth orientation. For instance, Wang *et al.* used various substrates for direct growth of a Co-TDC-MOF by thermally evaporating a metal layer (Ni, Co, Cu, Ag or Ti) onto them before the solvothermal synthesis. With this procedure, they ensured the synthesis of highly oriented quasi-2D MOF arrays over the different materials, due to the preferred coordination of the carboxyl groups in the ligands with the metal layer.[89]

Other materials used in the assistance of direct growth of MOFs, that have shown to improve their performance and stability, are layered double hydroxides (LDHs)[90] and alumina thin films (deposited using another innovative technique, atomic layer deposition),[91] where both templates yielded highly oriented MOF thin films.

Different groups have shown that it is possible to directly compare the electrocatalytic performance of a MOF drop casted on an electrode and one directly grown over it. For example, Duan *et al.* tested a NiFe–2,6-naphtalenedicarboxilate MOF as a catalyst for electrochemical water splitting, and they found

that the overpotential for a current density of 10 mA cm^{-2} was significantly smaller for the MOF grown solvothermally over Ni foam (240 mV) than that of the bulk MOF deposited over a GC electrode (318 mV), hence, showing that the direct growth of the MOF resulted in a more efficient catalyst with excellent stability over time.[34]

c. Liquid phase epitaxy

Liquid phase epitaxy (LPE) is another, more specific, direct growth technique that can be used to prepare surface-mounted MOFs (SURMOFs), which are highly orientated and homogeneous MOF thin films synthesized directly over a substrate. This method has useful advantages like control of orientation, tunable thickness, and strong adhesion to the substrate's surface.[92,93]

The basic scheme of this method is that a pretreated substrate is immersed sequentially in different solutions of the MOF precursors by using an automatic pumping system, in a layer-by-layer fashion (Fig. 3d). It is possible to obtain a MOF with the same characteristics as the bulk material, although it has been shown that some pseudomorphs of MOFs that are not accessible through the usual solvothermal synthesis methods can be obtained through LPE.[94]

However, it is important to note that the pretreatment of the substrates used for LPE involves the growth of a self-assembled monolayer (SAM) on their surface, which are usually constructed with organic molecules bearing carboxylate and pyridine headgroups, to serve as two-dimensional nucleation sites.[95] This creates an insulating layer between the electrode surface and the MOF, which would increase the electrical resistance of the electrode and could hinder charge transfer. Nevertheless, this is a very powerful technique to tune the morphology and composition of the resulting SURMOF, as the chemical functionality of the deposited SAM can induce a preferred crystal orientation and inhibit growth for selective deposition.[96]

To our knowledge, few SURMOFs prepared by LPE have been tested as electrocatalysts. This, however, is a synthesis method that could be further explored since the strong bond between the MOF and the substrate must be advantageous for long-term electrolysis. Furthermore, having well-defined and highly oriented SURMOFs would be useful to establish relationships between the material's morphology and its catalytic performance, to study the effect in mass and charge transport through MOFs of different thicknesses, and to evaluate the catalytic performance of different facets.

d. Electrochemical methods

Different electrochemical approaches can be used in the preparation of MOF-based electrodes. The two most common methods are direct electrochemical synthesis over a substrate and electrophoretic deposition of a previously synthesized material onto the electrode surface.

The main advantages of these electrochemical methods over drop casting, are the elimination of the need for a binder and a better control of the thickness of the deposited layer. In a typical electrophoretic deposition procedure, an electrochemical cell with the suspended MOF and a supporting electrolyte is mounted, with two pieces of the same substrate of choice as the anode and the cathode. An appropriate potential is applied between the substrate electrodes for a determined amount of time, both of which are usually high (typically 50–100 V during 1–3 h). This yields MOF films that are tightly bound to the substrate, improving their electrical contact with the surface, which in turn improves their electrocatalytic performance.[97,98]

A more novel and promising approach is the direct electrochemical synthesis over the substrate, usually a metal foam or foil. This is a very accessible way to obtain MOF thin films tightly bonded to a conductive substrate without the need for a binder, which results in MOF electrodes with much higher conductivity and stability. These properties make them ideal for electrocatalytic applications, though one needs to bear in mind that there could be possible activity of the metal substrate contributing to the electrochemical current.

As shown in Fig. 3c, an electrochemical synthesis cell consists of two pieces of substrate that act as anode and cathode, immersed in a solution that contains all the precursors needed for the synthesis of the MOF: metal salts, organic linkers, and a supporting electrolyte. Unlike electrophoretic deposition, the potential applied is not too high (1.5–10 V) and synthesis times are usually in the order of seconds.[81]

To highlight the potential that electrochemical synthesis has for the development of more efficient MOF electrocatalysts, it is worth mentioning the work by Kang *et al.* They prepared the MFM-300(In) MOF using an electrochemical cell, with In foils as the electrodes immersed in a solution containing the organic linker and supporting electrolyte. They obtained a deposited system that is catalytically active for the CO2RR, with a maximum current density of 46.1 mA cm^{-2} and maximum faradaic efficiency (F.E.) towards the formation of HCOOH of 99.1% in acetonitrile, a performance that exceeds most of the MOF systems used for electrocatalysis so far and it is clearly superior to that of the In foil by itself.[99] Despite these promising results, not many MOF catalysts for the CO2RR prepared by electrochemical synthesis have been reported, and this is a promising path that seems to remain largely unexplored.

4. Examples of MOFs catalyst for the CO2RR

The first report of a MOF used as a catalyst for the CO2RR was a Cu–rubeanic acid MOF in 2012.[100] Since then, several MOFs containing Cu, Zn, Fe, Re, Co and In and a variety of linkers have also been tested as catalysts for this purpose. Even if some of these materials have shown good electrocatalytic performance, selectivity, and stability, it is evident that C1 chemicals like CO are usually the main products of the MOF-catalyzed CO2RR systems, *versus* the more useful C2 chemicals like oxalates or ethanol.[101]

There are many ways that MOFs used as electrocatalysts for CO2RR systems can be classified. In this perspective, we focus

on the nature of the MOF linker to discuss their electrocatalytic performance towards the CO2RR.

• **Porphyrin linkers**

The typical porphyrin linker used in MOF catalysts towards the CO2RR has been the *meso*-tetra(4-carboxyphenyl)porphyrin (TCPP), on which a metal center is coordinated to the nitrogen atoms to act as active sites. The carboxylate groups in the porphyrin serve as coordination sites for the inorganic nodes to form the MOF's network. As seen in Table 1, different inorganic nodes, MOF configurations and metal incorporated to the porphyrin center have been tested. In addition, both aqueous and organic electrolytes have been used.

Among the metal centers that can be incorporated into the porphyrin linkers, Fe is a particularly interesting one, since it has been successfully used both in homogeneous catalysts and in nitrogen-doped carbon materials. A first example of a porphyrin and iron containing MOF was reported by Hod *et al.*[97] They tested electrodeposited Fe-MOF-525 films as a catalyst for the CO2RR in a 1 M $TBAPF_6$ acetonitrile solution, which is a high concentration of electrolyte that could facilitate the redox hopping mechanism. As shown in Fig. 4a, CO and H_2 were obtained as products in a controlled potential electrolysis experiment, with a F.E. of 54% for CO formation, though the MOF film showed degradation after 30 minutes.

The same main product in the CO2RR was obtained in the work by Dong *et al.*,[102] who synthesized a 3D PCN-222(Fe) MOF, $[Zr_6O_8(OH)_4(H_2O)_4][(TCPP–Fe-(III)–Cl)_2]$, that consists of the same building blocks as MOF-525 but has a different spatial arrangement, resulting in a star-shaped network of Zr_6 clusters linked by square-planar Fe–TCPP fragments. Its peak performance was reached at −0.60 V *vs.* RHE (η = 494 mV), for a maximum CO F.E. of 91% in a 0.5 M $KHCO_3$ aqueous solution (Fig. 4b). This lower onset overpotential than the one observed in Fe-MOF-525 could be a result of better mass transport through the PCN-222 channels, the improved conductivity in the presence of carbon, and the higher availability of protons when working in an aqueous electrolyte. Interestingly, the selectivity towards the competing process remains low, despite working in a protic medium, showing that, under the right conditions, the FeN_4 sites can be extremely selective towards CO formation. In a long term chronoamperometric operation (at −0.60 V *vs.* RHE for 10 h), however, the average CO FE dropped to 80.4% over the entire period, showing that stability still needs to be improved.

In addition to Fe, another common metal that is efficient for the reduction of CO_2 into CO on porphyrin-based catalysts is Co. Therefore, it is not surprising that MOFs containing Co porphyrins show high CO faradaic efficiency, as in the previously discussed work of Xin *et al.*, who reported a remarkable CO faradaic efficiency of 97% using MOF-545-Co doped with cobaltocene.[50] Previously, Kornienko *et al.* had studied the effect of the metal center on a family of M–TCPP MOFs.[91] In their work, the metalated porphyrins were assembled into a 3D

Table 1 MOF systems containing porphyrinic units as organic linkers tested as electrocatalysts for the CO2RR

Metal center	MOF	Electrolyte	Potential	Main product	Max FE (%)	Ref.
Co (Cu, Zn)	$[Al_2(OH)_2TCPP-M']$	0.5 M $KHCO_3$	−0.7 V (*vs.* RHE)	CO	76	91
Cu	Cu_2(CuTCPP) (nanosheets)	0.5 M $EmimBF_4$ (CH_3CN)	−1.2 V (*vs.* Ag/Ag^+)	$HCOO^-$, CH_3COO^-	85	82
Fe	Fe-MOF-525	1 M $TBAPF_4$ (in DMF)	−1.3 V (*vs.* NHE)	CO	54	97
Fe	PCN-222(Fe)	0.5 M $KHCO_3$	−0.6 V (*vs.* RHE)	CO	91	102
Co	$CoCp_2$@PCN-222-Co	0.5 M $KHCO_3$	−0.7 V (*vs.* RHE)	CO	97	50

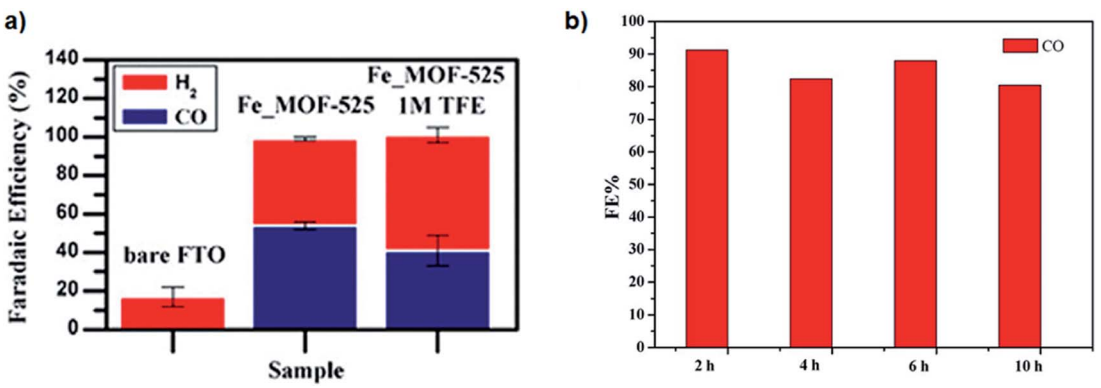

Fig. 4 Electrocatalytic results on two different Fe–TCPP based MOFs, MOF-525 (ref. 97, (a)) and PCN-222 (ref. 102, (b)). (a) Faradaic efficiency of Fe-MOF-525 towards the main products in each electrolysis condition (reproduced with permission from ref. 97. Copyright American Chemical Society 2015, further permissions related to the material excerpted should be directed to the ACS) and (b) faradaic efficiency of Fe-PCN-222 towards CO formation over time (adapted with permission from ref. 102. Copyright 2018 American Chemical Society).

MOF through reacting on an alumina coated electrode, prepared by ALD. Zn, Cu and Co MOFs were synthesized and probed as electrocatalysts for the CO2RR, yet only the Co MOF showed good performance and stability in equal conditions, with a maximum F.E. towards the formation of CO of 76% and a stable current through 7 h of continuous electrolysis at −0.7 V *vs.* RHE.

Another metal center used in CO2RR catalysts has been copper, perhaps due to its remarkable catalytic activity as a metal. However, it is important to ensure that the metal is indeed an isolated site and that no nanoparticles are formed. This was unfortunately the case in the work by Wu *et al.* on the Cu_2(CuTCPP) MOF, which is a porous 2D layered network with $Cu_2(COO)_4$ paddle wheels as the connecting elements. In their study, it was proven that the MOF itself was not the active catalyst, but instead other Cu species generated *in situ* by the electrolysis process.[82] Therefore, a previous electrolysis of the catalyst at −1.55 V was necessary to activate it to reach its maximum activity with a FE of 68.4% and 16.8% at −1.55 V *vs.* Ag^+/Ag for formate and acetate production, respectively. These results highlight the importance of characterization of the catalyst material after reaction since, as discussed in Section 2, MOFs' structure can evolve significantly under electrochemical conditions.

While the CO2RR studies on porphyrin-based MOFs have been focused on TCPP, there are other kinds of porphyrin-metal systems known to be efficient homogeneous catalysts. It has been observed that changing the substituents on the porphyrin's phenyl groups alters the electronic density of the metal center, which can be used to tune the efficiency and selectivity of an homogeneous catalyst.[103] A similar approach could be employed in the study of electrocatalytic MOFs to enhance their performance, by incorporating different functional groups in the porphyrinic linker and establishing relations between the electronic properties of the substituent and catalytic performance.

• Aromatic linkers

Trimesic acid (benzene-1,3,5-tricarboxylic acid, BTC) is a classic aromatic linker used in the synthesis of MOFs with different morphologies, like the HKUST-1 family. As it is evident in the examples presented in Table 2, despite having the same organic linker, factors like metal center, morphology, electrode preparation, and working electrolyte have great influence in the BTC MOFs' catalytic performance. It has been demonstrated that this family of MOFs can generate a wide variety of products during the CO2RR reaction, including CO, formate, methane, and alcohols. Unfortunately, there has not been an extensive effort to observe any kind of trend in their electrocatalytic performance, which would be needed to have a better understanding of the role that the formerly mentioned factors have in the catalytic process.

A direct comparison can be made between the work of Albo *et al.* and Perfecto *et al.* They both tested the same system, (Cu) HKUST-1, in gas diffusion electrodes (GDE) prepared by air-brushing the catalyst ink over carbon paper,[84,85] and observed production of alcohols. The electrocatalytic activity of both MOFs was tested under similar rection conditions and showed comparable stability and product selectivity, but it was evident that doping the MOF with other metal centers like Ru creates a synergistic effect that dramatically enhances its catalytic activity.[85]

Other BTC MOFs have been tested as electrocatalysts for the CO2RR, however, the morphology, synthesis method, metal center and electrolysis conditions in these MOFs are widely different. Therefore, as expected, their electrocatalytic performance, stability and product selectivity are different as well. The importance of the reaction medium can be appreciated in the work by Kang *et al.* (Fig. 5a), who synthesized a Zn-BTC MOF by mixing different mole fractions of $ZnCl_2$ with BTC in a mixed solvent consisting of 75% 1-dodecyl-3-methylimidazolium chloride (C_{12}mimCl) and 25% glycerol. The $ZnCl_2$ content in the reaction medium had great influence on the morphology of the obtained MOF, and therefore on its electrocatalytic activity. The sheet-like Zn-MOF synthesized at $x = 0.38$ showed the best performance and stability, with a F.E. of 80.1% towards the formation of CH_4 at 2.2 V (*vs.* Ag/Ag^+) in an ionic liquid (1-butyl-3-methylimidazolium tetrafluoroborate ($BmimBF_4$)) medium, which proved to be crucial in the high faradaic efficiency and selectivity.[98]

A more innovative synthetic method was explored by Kang *et al.* The electrochemical synthesis of MFM-300(In) was carried out in a solution of biphenyl-3,3′,5,5′-tetracarboxylic acid, with In foil as anode, cathode, and metal ion source at an applied potential of 10 V at 60 °C for 200 s. The conductive nature of the electrode substrate resulted in a remarkable catalytic performance with a very high faradaic efficiency of 99.1% for formic acid formation at −2.15 V (*vs.* Ag/Ag^+).[99] The importance of electrode preparation can be seen clearly in Fig. 6. As

Table 2 MOF systems containing aromatic molecules as organic linkers tested as electrocatalysts for the CO2RR

Metal center	MOF	Electrolyte	Potential	Main product	Max FE (%)	Ref.
Re	$ReL(CO)_3Cl$ (L = 2,2′-bipyridine-5,5′-dicarboxylic acid) (SURMOF)	0.1 M TBAH (CH_3CN)	−1.6 V (*vs.* NHE)	CO	93	93
Cu	$Cu_3(BTC)_2$	0.01 M $TBABF_4$ (DMF)	−2.5 V (*vs.* Ag/Ag^+)	$H_2C_2O_4$	51	38
In	MFM-300(In)	0.5 M $EmimBF_4$ (CH_3CN)	−2.15 V (*vs.* Ag/Ag^+)	HCOOH	99	99
Zn	ZnBTC-MOF	$BmimBF_4$	−2.2 V (*vs.* Ag/Ag^+)	CH_4	80	98
Cu	(Cu)HKUST-1	0.5 M $KHCO_3$	−0.9 V (*vs.* RHE)	MeOH	15	84
Cu + Ru	(Cu,Ru)HKUST-1	0.5 M $KHCO_3$	−1.1 V (*vs.* Ag/Ag^+)	MeOH, EtOH	47	85
Zn	Zn-MOF-74	0.5 M $KHCO_3$	−0.91 (*vs.* RHE)	CO (H_2)	15	104

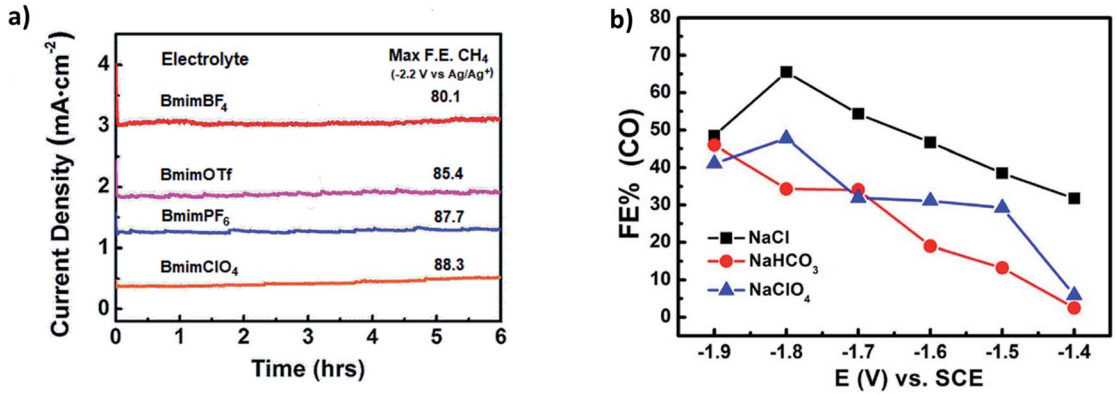

Fig. 5 Influence of the support electrolyte in MOFs' electrocatalytic performance. (a) Performance of a Zn-BTC MOF (ref. 98) in various ionic liquids used as support electrolytes in a controlled potential CO_2 electrolysis. (Reproduced from ref. 98 with permission from the Royal Society of Chemistry). In (b), the faradaic efficiency of CO production as a function of applied potential is plotted for a Zn-ZIF-8 system (ref. 73), in various aqueous electrolytes (reproduced with permission from ref. 73, ©2017 Wiley-VCH Verlag GmbH & Co. KGaA, Weinheim).

mentioned in Section 2, it is possible to compare and observe clear differences in the electrocatalytic performance of the same MOF system depending on the construction method of the electrode. Among the tested methods, electrochemical synthesis over an In foil resulted in a better catalytic performance when compared with electrochemical synthesis followed by deposition over carbon paper, and drop casting over carbon paper of the solvothermally prepared MOF.

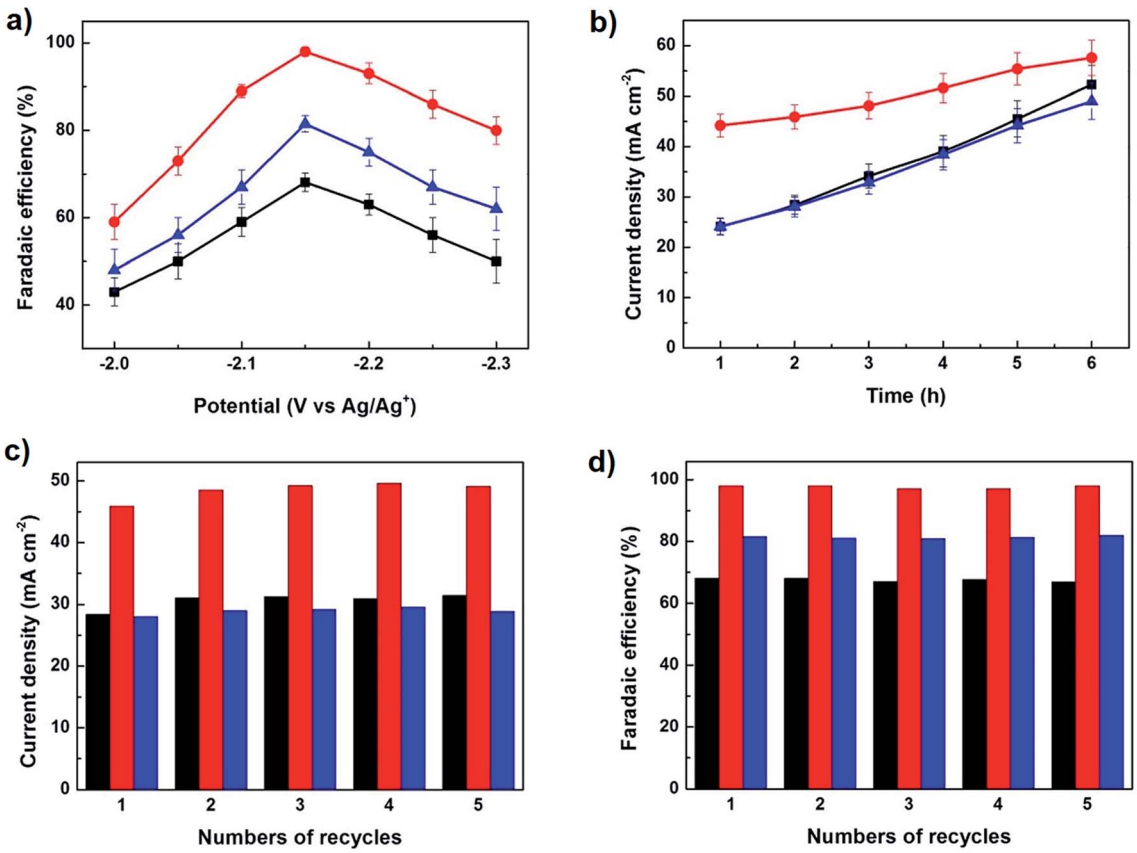

Fig. 6 Electrochemical CO2RR performance of MFM-300(In) prepared *via* different synthesis methods by Kang *et al.* (ref. 99): electrochemical synthesis over an In foil (red), electrochemical synthesis followed by deposition over carbon paper (blue) and solvothermal synthesis and drop casting over carbon paper (black). (a) Shows faradaic efficiency towards the formation of HCOOH, (b) plots the current density in a constant potential electrolysis, and (c) and (d) convey the change in current density and faradaic efficiency in five cycles of a 2 h constant potential electrolysis at −2.15 V (*vs.* Ag/Ag^+) (reproduced with permission from ref. 99. Copyright American Chemical Society 2020, further permissions related to the material excerpted should be directed to the ACS).

The use of metal foils or foams as substrates to prepare MOF-based electrodes for electrocatalysis is an approach previously explored in other systems for reactions of interest like OER[90,92,105] but, to the best of our knowledge, this is the first work that explored this promising method for the synthesis of an electrocatalytic MOF species for CO2RR. It is important to keep in mind, however, that the ideal metal to be used as substrate in these types of conductive MOF-based electrodes should not be active towards the CO2RR, to ensure that the observed catalytic activity is indeed attributed to the MOF.

• **ZIF type MOFs**

ZIFs are a subclass of MOFs (zeolitic imidazolate frameworks) with zeolite topology constructed from imidazolate ligands and metal ions, that exhibit good stability in aqueous media. As it can be seen in Table 3, one of the first works exploring their use as possible electrocatalysts for the CO2RR was the one by Wang *et al.*, where they chose ZIF-8 due to its previously reported high CO_2 adsorption properties.[73] They also tested the effect of the counterion of the Zn source and the supporting electrolyte used during the electrocatalytic test. Using $ZnSO_4$ as the Zn source in synthesis yielded small rhombic dodecahedral crystals (~150 nm), which presented the highest faradaic efficiency and the broadest potential range suitable for CO_2 reduction. Additionally, the supporting electrolyte played a crucial role on the catalyst efficiency (Fig. 5b). The best results were observed using NaCl as electrolyte, and these positive results are attributed to the smaller Cl^- anion hydrated radius, that probably leads to a more efficient anion transfer. As we discussed in Section 2, this is important to ensure an efficient charge transfer throughout the MOF structure *via* the redox-hopping mechanism. NaCl, however, is not an ideal candidate to be used as a supporting electrolyte. On one hand, Cl^- can be oxidized at the anode to form Cl_2, which is highly corrosive. In addition, working in a non-buffer electrolyte can lead to important pH changes (particularly at the interphase), which could interfere with the reaction's selectivity.[106]

After the work from Wang *et al.*, other reports have shown high selectivity for CO production using Zn-ZIF catalysts. For instance, Jiang *et al.* tested various Zn-ZIF systems: ZIF-7, ZIF-8, ZIF-108, which share the same sodalite topology but differ from each other in the imidazole species used as the organic linker to construct them.[75] They found the Zn-ZIF-8 species to be the most active and ZIF-7 the least active.

In addition, as shown by Dou *et al.*, the presence of a different ligand can modify the catalytic performance of the MOF. They activated a Zn-ZIF-8 sample through heating at 250 °C for 3 h, to generate Zn open sites. Afterward, 1,10-phenanthroline was added and its N atoms coordinated to the Zn open sites. They reported a F.E. towards the production of CO of 54% for the pristine Zn-ZIF-8, and an increased CO selectivity after doping, to achieve a maximum F.E. of 91%. The improved performance of the doped material is attributed to the presence of a stronger electron-donating species, facilitating CO_2 activation at the catalyst's active sites.[72] These results are a good example on how the activity of MOFs can be tuned by introducing new ligands in their structure and modifying its overall electronic properties, which, as we discuss in Section 5, is a strategy that can be further explored for catalyst optimization.

As of now, the $Ni(Im)_2$ ZIF nanosheet system studied by Wu *et al.* is the only non-Zn ZIF probed as an electrocatalyst for the CO2RR. The maximum faradaic efficiency of 79% for the production of CO was achieved only until the bulk $Ni(Im)_2$ was exfoliated into nanosheets ~5 nm thick. As the thickness of the catalyst increased, the F.E. decreased until it reached the minimum F.E. of 34% observed in the bulk ZIF.[74] Additionally, despite the use of ultra-thin nanosheets as the electrocatalyst, it showed good stability over time even in long-term electrolysis experiments. These observations show that for MOF-based catalysts there are many important parameters to optimize. While the structure of the active site is indeed crucial, the morphology and thickness of the deposited films are also important. In this case, an increase in superficial active site density is observed when the catalyst films are thinner, since a thick film might limit mass transport, reducing the number of available active sites. As previously mentioned, charge transfer in MOFs also requires the diffusion of counter ions to balance the charge of redox hopping, so limiting ion transfer might also have a negative impact on the electrocatalytic performance.

• **Phthalocyanine linkers**

The use of phthalocyanines as building blocks for MOFs is one of the newer and most promising approaches in the search for a MOF system that can be used as an efficient CO2RR electrocatalyst. It is noteworthy that phthalocyanines are structurally related to porphyrins, and they also possess an extensively delocalized π electron system that, together with d–π and π-stacking interactions, offer a possibility to overcome the issue of low electrical conductivity.[64] As it can be seen in Table 4, the use of MOFs with phthalocyanine linkers has resulted in highly selective catalysis towards CO production in aqueous electrolytes.

One of the first studies using phthalocyanine linkers was carried out by Zhang *et al.*, who studied a Ni phthalocyanine-

Table 3 ZIF-MOF systems tested as electrocatalysts for the CO2RR

Metal center	MOF	Electrolyte	Potential	Main product	Max FE (%)	Ref.
Zn	ZIF-8-phen	0.1 M $KHCO_3$	−1.1 V (*vs.* RHE)	CO	90	72
Ni	$Ni(Im)_2$ ZIF	0.5 M $KHCO_3$	−0.85 V (*vs.* RHE)	CO	79	74
Zn	ZIF-8	0.25 M K_2SO_4	−1.1 V (*vs.* RHE)	CO	81	75
	ZIF-7				24	
Zn	ZIF-8	0.5 M NaCl	−1.8 V (*vs.* SCE)	CO	66	73

Table 4 Phthalocyanine-based MOF systems tested as electrocatalysts for the CO2RR

Metal center	MOF	Electrolyte	Potential	Main product	Max FE (%)	Ref.
Ni	NiPc–Ni(NH)$_4$	0.5 M $KHCO_3$	−0.7 V (*vs.* RHE)	CO	96	107
Zn	PcCu–O_8–Zn	0.1 M $KHCO_3$	−0.7 V (*vs.* RHE)	CO	88	108
Co	CoPc–Cu–O	0.2 M $KHCO_3$	−0.74 V (*vs.* RHE)	CO	85	64
Ni	NiPc–NiO_4	0.5 M $KHCO_3$	−0.85 V (*vs.* RHE)	CO	98.4	63
Co	MOF-1992	0.1 M $KHCO_3$	−0.63 V (*vs.* RHE)	CO	78	109

based MOF as an electrocatalyst for the CO2RR. The NiPc-Ni(NH_4) nanosheets exhibited good performance and selectivity towards the formation of CO, with no morphology changes after 10 h of electrolysis, confirming that the catalytic active sites were the Ni-Pc motifs. These results show the potential of using Ni as a metal center in MOF-based catalysts, which despite being commonly used in carbon-based materials, has not been widely explored in MOF-based electrodes.[107]

In a more recent study, Yi *et al.* prepared a Ni-Pc-NiO_4 MOF *via* solvothermal synthesis and exfoliated the bulk powder into 5-layer 2D nanosheets through sonication, to obtain a highly conductive MOF (4.8×10^{-5} S m^{-1}).[63] Consistently with Zhang *et al.*,[107] they observed high CO selectivity (F.E. of 98.4% at −0.85 V) and, using DFT (Density Functional Theory) calculations, they proposed that the active catalytic site is the NiN_4 moiety in the NiPc. Interestingly, the isolated phthalocyanine also has some electrocatalytic activity, which is significantly enhanced when it is fixed as part of the MOF structure (Fig. 7). These results highlight the importance of having a holistic approach when designing MOF-based catalysts. Combining the presence of highly active sites, such as NiN_4, with the conductive MOF structure resulted in a MOF with a remarkable catalytic performance.

As with other types of linkers, Co has also proven to be an interesting metal center to be used as an active site in phthalocyanine-based MOFs, as it was shown in the work of Matheu *et al.* They prepared an anionic metal-catecholate MOF, MOF-1992, aiming to have a favorable orbital overlap between the metal ion and the catechol, to facilitate charge transport. The amount of electroactive species of the MOF deposited over a glassy carbon electrode was very high (270 nm cm^{-2}), when compared to the electroactive coverage of MOFs based on Zr or Al nodes. Thus, this system showed a F.E. towards CO formation of 78% (21% for H_2) and an average current density of −16.5 mA cm^{-2} at −0.63 V *vs.* RHE, one of the highest for MOF-based cathodes at similar working potentials.[109]

Another work on conductive MOFs was recently published by Meng *et al.*, using a series of MPc–Cu–X MOFs, where X represents a bis(diamine) or bis(dioxolane) crosslinker. The Cu nodes are considered inactive towards the CO2RR, so the observed activity is attributed to the M-Pc moieties. Interestingly, when comparing Ni and Co, the latter shows better catalytic performance, reaching a maximum current density of −9.5 mA cm^{-2} and a F.E. towards CO formation of 79%. These results were improved by forming a composite with a conductive additive like carbon black (CO FE 85% with a peak current density of −13.2 mA cm^{-2}) showing that, despite the high intrinsic conductivity of this MOF (2.12×10^{-2} S cm^{-1}), it can be increased further to yield better catalytic results. The observed experimental trends were consistent with DFT calculations, which showed that the CoPc–Cu–O species has the lowest energy barrier (0.63 eV) for the rate limiting step, namely, the formation of the *COOH intermediate on the MOF.[64]

As we will discuss in the next section, DFT calculations can be useful to understand trends within a family of MOFs, as was done by Meng *et al.* In addition, it can be a powerful tool for the rational design of electrocatalysts. This was the approach explored by Zhong *et al.*, who used DFT calculations to optimize the possible phthalocyanine MOF catalyst before any synthesis attempts. Among the studied candidates, PcCu–O_8–Zn showed the lowest Gibbs energy for the *COOH intermediate formation. These theoretical observations were proved experimentally, as

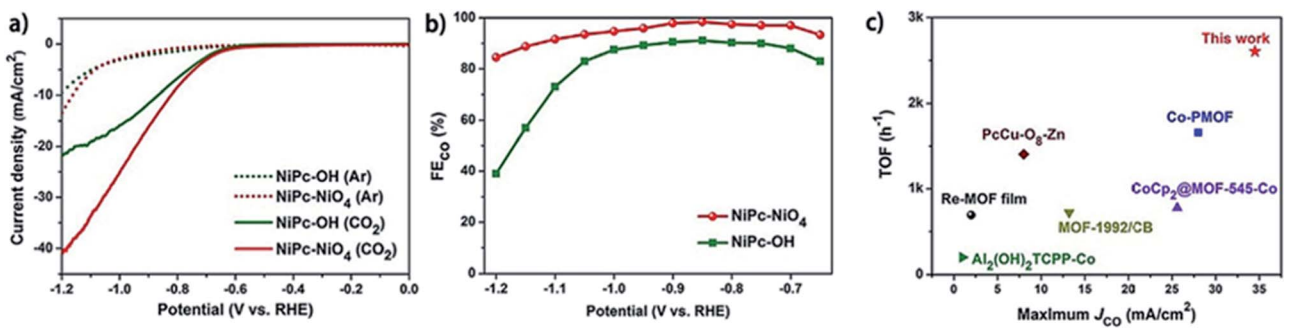

Fig. 7 Electrocatalytic performance of the NiPc-NiO_4 MOF system *vs.* isolated Ni-Pc (ref. 63). (a) LSV curve comparison in Ar and CO_2 saturated electrolyte. (b) Faradaic efficiencies towards CO formation. (c) Performance comparison *vs.* other reported CO2RR electrocatalytic systems (reproduced with permission from ref. 63, ©2021 Wiley-VCH GmbH).

Table 5 MOF systems containing various molecules as organic linkers tested as electrocatalysts for the CO2RR

Metal center	MOF	Electrolyte	Potential	Main product	Max FE (%)	Ref.
Cu	CR-MOF	0.5 M $KHCO_3$	−1.2 V (*vs.* SHE)	HCOOH	30	100
Cu	Cu–ade-MOF	0.1 M $KHCO_3$	−1.6 (*vs.* RHE)	CH_4, C_2H_4	73	79
Cu	Cu-THQ	1 M $C_5H_{14}ClNO$ + 1 M KOH	−0.45 (*vs.* RHE)	CO	91	110

the PcCu–O_8–Zn/CNT composite yielded the highest F.E. towards the formation of CO (88% at −0.7 V *vs.* RHE), the lowest Tafel slope and the smallest resistance. In addition, *operando* studies using XAS (X-ray adsorption spectroscopy) and SEIRA (surface-enhanced IR absorption spectroelectrochemistry) confirmed that the M–O_4 nodes are the active sites of these materials.[108]

- **Miscellaneous linkers**

Finally, presented in Table 5, are studies that deal with MOFs that do not correspond to the previously mentioned families of organic linkers, but are worth mentioning. Such is the case of the work from Hinogami *et al.* Despite the low faradaic efficiency observed on their Cu–rubeanic acid MOF, it is a significant study because it is the first report of a MOF used as a catalyst for the electrochemical CO2RR. Additionally, the use of rubeanic acid (dithiooxamide) as a linker stands out as different to other typical MOF linkers used in catalyst synthesis, since it is a relatively small and non-aromatic amide. The results, which can be seen in full in Fig. 8, indicate that this MOF is capable of reducing CO_2 into formic acid, with a maximum F.E. of 30%, and good stability in electrolysis, showing some potential as a catalyst for the CO2RR.[100]

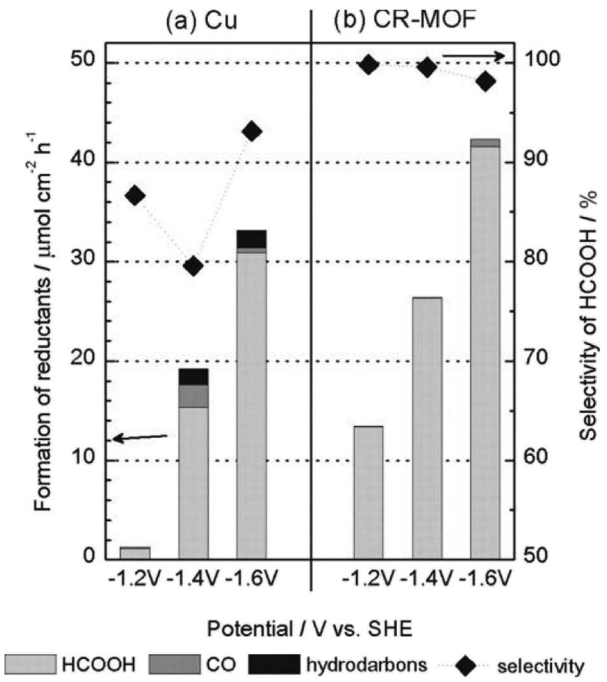

Fig. 8 Contrast between the electrocatalytic performance and selectivity of Hinogami *et al.* (ref. 100). Cu–rubeanic acid MOF and a Cu electrode (ref. 100, ©The Electrochemical Society. Reproduced by permission of IOP Publishing Ltd all rights reserved).

Another copper-based MOF recently reported is a Cu–adenine MOF with nanosheet morphology, reported by Yang *et al.* This MOF is prepared by the coordination of Cu^{2+} ions to adenine and acetic acid. Interestingly, this material showed direct reduction of CO_2 into hydrocarbons, with selectivity towards ethylene and methane production at −1.4 V and −1.6 V *vs.* RHE, respectively.[79] However, it was noted that the morphology of the MOF was essentially destroyed after electrolysis, with TEM images indicating Cu nanoparticle agglomeration. Consequently, it was concluded that the actual active sites were these Cu clusters with some C and N motifs instead of the original MOF structure. This denotes the importance of systematic structural studies of MOFs before and after electrolysis, to confirm that the catalytic processes observed are being carried out by the actual MOF structure and not a derived material.

A remarkable and novel study is the one conducted by Majidi *et al.*, where they report the synthesis of a 2D conductive copper–tetrahydroxyquinone MOF. This is a good example of a different conductive MOF that can be used in electrocatalysis. The bulk MOF was converted into nano-flakes by a liquid-phase exfoliation method, and they were loaded onto a GDE for the electrochemical tests. This system showed an outstanding performance, exhibiting the highest current density and lowest overpotential reported to date (160 mA cm^{-2} at 16 mV of overpotential), with selective CO formation even at this remarkably low overpotential. The high selectivity of the system towards CO formation was studied *via* DFT calculations. It was shown that the formation of the *CHO intermediate, which is commonly considered to be the key intermediate for methane and methanol production, becomes more favorable at a more negative overpotential, thus working at a low overpotential favors CO formation, while a more negative potential will favor more reduced products.[110] In addition, working with a GDE reduces mass transport limitations, and using an alkaline electrolyte inhibits the competing process of the HER. Therefore, a fair comparison of different MOF catalysts should be carried out under the same conditions.

5. Structure–activity relations

As discussed in the previous sections, MOF-based electrodes have shown encouraging results as electrocatalysts for the CO2RR. Nevertheless, the structure–activity relations are still not well understood. Therefore, extensive studies on the role of key structural parameters such as the nature of the metal, its coordination environment and the electronic properties of the

linker are still needed. Ideally, those studies should be accompanied by computational simulations to estimate the binding energies of the key reaction intermediates to the MOF's active sites (*H, *COOH, *CO and *CHO), since these serve as descriptors to predict the activity and selectivity of the catalytic process.[6]

In particular, combined theoretical and experimental studies have shown that the selectivity of MNC catalysts is dependent on the nature of the metal incorporated to the carbon matrix, which is attributed to the difference in binding energy between the active metal and the reaction intermediates.[111,112] Similar to metal catalysts, *COOH binding energy can be used as a descriptor for the onset potential of the CO2RR, whereas a stronger *H adsorption, resulted in higher HER activity and lower CO selectivity.[112]

Such combined experiment–theory studies to understand the role of the metal center in MOF-based catalysts are still limited. In this regard, it is worth mentioning the work by Meng *et al.*, who used DFT calculations to explain the difference in catalytic activity between the Ni and Co 2D MOFs made of metal-phthalocyanine (MPc) linkers and Cu nodes.[64] Their results show a lower activation energy for the formation of the carboxyl intermediate (*CHOO) in the CoPc-based MOF, in comparison with NiPc, which is consistent with its higher activity and selectivity for CO formation. In addition, different groups have used computational screening to predict the activity of different MOF-based catalysts towards the CO2RR. For this approach, the binding energy of intermediates and the calculated Gibbs energy of each step of the reaction mechanism can be used to elucidate a catalyst's activity and product selectivity. For instance, Xing *et al.* use the binding energy between the metal center and reaction intermediates to determine the rate-limiting step on a series of two-dimensional metal hexahydroxybenzene frameworks $M_3(HHB)_2$; and, based on this analysis, they identified $M_3(HHB)_2$ (M = Cr, Mo, Ru, and Rh) as the most promising candidates for CO2RR catalysis.[113] Moreover, they also predict that the main reduction product will depend on the metal center, with CH_4 being the main product on Cr and Mo, while CH_3OH is expected on Ru and Rh. Similarly, Tian *et al.*[114] evaluated the potential electrocatalytic activity towards the CO2RR of the 2D conductive MOFs $M_3(HITP)_2$, M = Fe, Co, Ni, Ru, Pd and Rh, which were previously mentioned in Section 2. They first used the calculated value of the *CO intermediate adsorption energy to evaluate the possibility of obtaining further reduced products, and then a free energy profile of the reduction mechanism was obtained for each catalyst. Their results suggest that, for M = Fe, Co and Rh, the MOFs will be catalytically active towards the CO2RR and will yield methanol as the main product. Particularly, $Ru_3(HITP)_2$ is the only one predicted to have selectivity towards methane production.

In addition to using the binding energy of intermediates, the d band center can also be used as a descriptor,[115] as was done by Mao *et al.* They studied another $M_3(HITP)_2$ MOF series, where M= Ti to Cu, and found the MOF containing FeN_4 sites to be the most active one for the selective conversion of CO_2 to CH_4.[116] Interestingly, these theoretical studies suggest the formation of highly reduced products, which are attractive products, yet there are only few MOFs that experimentally reduce CO_2 into CH_4 and CH_3OH. Moreover, the two mentioned studies focusing on $M_3(HITP)_2$ MOFs have discrepancies in some of the proposed reaction products and selectivity. Therefore, it would be desirable to carry out experiments to corroborate these predictions and get further insight on the structural parameters that control the selectivity of the CO2RR.

The key role of metals also provides us the opportunity to use multi-metal MOFs to enhance their catalytic performance. Having two distinct active sites can create a tandem catalyst, in which the first reaction steps take place on one site and the reaction is completed on another. This approach was used by Choukroun *et al.* to have an efficient reduction of CO_2 to CO on Ni single sites, followed by CO reduction into hydrocarbons on copper nanoparticles.[117] Moreover, the two metals could be playing a synergistic effect to facilitate the catalytic process. For example, Zhong *et al.* used a bimetallic MOF with copper–phthalocyanine ligands (CuN_4) and a Zn complex (ZnO_4) as linkage, and proposed a synergistic catalytic mechanism in which the ZnO_4 nodes act as the CO2RR catalytic sites while the CuN_4 centers promote the CO2RR.[108]

More interestingly, the two metals could be involved in the same active site and modulate its electronic structure. This strategy can be used to optimize the adsorption of reaction intermediates, thus favoring the desired reaction. In this regard, MOFs containing heterometallic units as active sites have shown encouraging results for other electrocatalytic processes[118,119] but, to our knowledge, they have not been probed for the CO2RR. This is a promising option to explore, as dual isolated metal sites on MNC materials have already shown to be highly efficient for the CO2RR.[120] Furthermore, multi-metal sites present an opportunity in the development of new catalysts for the production of multi-carbon products, as adjacent active sites to bind the *CO intermediates are needed to promote their formation.

While most studies directed to establish structure–activity correlations have focused on the effect of the metal center on the activity of single-atom catalysts, its coordination environment also plays a crucial role. As was shown in the study by Yuan *et al.*, for metal sites dispersed on graphene, carbon–nitride coordination leads to higher CO2RR electrocatalytic activity compared to phosphorus and sulfur coordination.[121] Similarly, in the case of MOFs, the intrinsic activity of a metal can be tuned by the nature of the linker, as it can affect the electronic density on the metal site.[122] For instance, as mentioned in the previous section, doping a Zn-ZIF-8 MOF with a stronger electron-donating species (1,10-phenantroline) resulted in a higher F.E. towards CO formation.[72] Furthermore, the ligand might also directly participate in the catalytic process, as proposed by Jian *et al.* for a family of Zn-ZIF catalysts that share the same topology, but have distinct imidazoles as organic linkers.[75] They found that having a different linker clearly changed the selectivity of the catalyst. This observation, along with DFT calculations, led to the conclusion that the active sites in this type of catalysts are actually the sp^2 C atoms from the imidazolate ligands, showing the complexity of these

systems in which more than one active site might be present. Therefore, a holistic approach to understand all the possible factors that affect the catalytic performance of MOFs is needed to optimize their catalytic performance.

6. Outlook

Metal–organic frameworks are versatile, high surface area materials that have shown promising performance in different electrocatalytic processes including the CO2RR. A key advantage of MOFs over other heterogeneous catalysts is the presence of well-defined single-atom sites, which can be fully characterized to establish structure–activity correlations. Hence, the study of pristine MOFs as electrocatalysts for the CO2RR is an interesting strategy to gain insight into the structural parameters that affect the catalytic performance of single-atom sites, to design more efficient CO_2 reduction catalysts.

Despite the promising early results of MOFs as electrocatalysts, there are still important challenges to overcome. Namely, the poor conductivity of MOFs and their limited stability under reaction conditions. To overcome the first issue, composites of MOFs with conductive materials is an attractive approach to be further explored, nevertheless, improving the intrinsic conductivity of MOFs is still desired. In this regard, it is important to consider the size of the MOF channels and counter ions, and the properties of the redox sites to optimize charge transfer *via* redox hopping. Alternatively, the design of conductive MOFs presents a promising opportunity for the development of efficient MOF-based electrocatalysts.

Another key challenge is the stability of MOF-based electrodes, which is affected by its preparation method and the structure and composition of the MOF. While drop casting of inks is a facile and versatile option for preparing MOF-based electrodes, it also has important drawbacks. For instance, the resulting physical attachment between the MOF and the substrate tends to be unstable. Therefore, the use of alternative preparation methods such as electrodeposition and direct growth, which result in chemical bonding between the MOF and the substrate, are highly desired. Having a strong MOF attachment to the electrode surface, however, does not guarantee long-term stability since the integrity of the MOF structure can also be affected by the supporting electrolyte and the current flow. In this regard, it is important to consider the stability of the MOF in aqueous electrolytes and in the presence of bicarbonate ions, which is the preferred medium to carry out CO_2 electrolysis. Likewise, the chemical stability of the MOF might be affected by the applied potential for electrolysis. Therefore, future applications of MOFs for CO2RR electrocatalysis will depend on the development of stable MOFs under these conditions. To corroborate the stability of MOFs, the studies of their catalytic performance should be accompanied by extensive material characterization, either *operando* or after reaction, to ensure the MOF structure is maintained under reaction conditions.

Despite these challenges, a variety of MOFs, synthesized with different families of linkers and metal centers, have been successfully utilized as electrocatalysts for the CO2RR, showing that they can reduce CO_2 into CO, formic acid and even hydrocarbons and alcohols. While these studies indicate that the performance of MOF-based catalysts can be tuned by the supporting electrolyte or the metal center, systematic studies of how different parameters affect the catalytic performance of MOFs are still needed. Future studies should take advantage of the tunability of MOFs to elucidate the role of the active metal center, pore size or substituent on the linkers to design optimal catalysts. In addition, the use of MOFs containing multi-metal sites presents an opportunity to further tune their catalytic activity. This is caused by the presence of adjacent active sites within the structure, which impacts the binding energy of reaction intermediates and can also lead to the formation of highly desired multi-carbon products, by facilitating carbon–carbon coupling.

In order to establish clear relations between the structure and the activity of MOF-based electrodes, it will be necessary to have a holistic approach. The measurements of catalytic performance should be accompanied by extensive characterization. *Operando* techniques, in particular, will be fundamental for the understanding of the nature of the active site under reaction conditions. Furthermore, theoretical studies can be used to further characterize the role of the metal center and linker, by determining the strength of the interaction between the catalysts and reaction intermediates. This information is essential to elucidate and understand the reaction mechanism, identify the rate-limiting step and to predict optimal active sites. Then, the complete outlook of these systems can be used as a solid starting point in the design of more efficient catalytic materials.

Conflicts of interest

There are no conflicts to declare.

Acknowledgements

This work is part of the Berkeley Global Science Initiative and received funding from PAPIIT (project number IA202819).

References

1 J. Davis Steven, S. Lewis Nathan, M. Shaner, S. Aggarwal, D. Arent, L. Azevedo Inês, M. Benson Sally, T. Bradley, J. Brouwer, Y.-M. Chiang, T. M. Clack Christopher, A. Cohen, S. Doig, J. Edmonds, P. Fennell, B. Field Christopher, B. Hannegan, B.-M. Hodge, I. Hoffert Martin, E. Ingersoll, P. Jaramillo, S. Lackner Klaus, J. Mach Katharine, M. Mastrandrea, J. Ogden, F. Peterson Per, L. Sanchez Daniel, D. Sperling, J. Stagner, E. Trancik Jessika, C.-J. Yang and K. Caldeira, *Science*, 2018, **360**, eaas9793.

2 A. Al-Mamoori, A. Krishnamurthy, A. A. Rownaghi and F. Rezaei, *Energy Technol.*, 2017, **5**, 834–849.

3 Y. Y. Birdja, E. Pérez-Gallent, M. C. Figueiredo, A. J. Göttle, F. Calle-Vallejo and M. T. M. Koper, *Nat. Energy*, 2019, **4**, 732–745.

4 X. Lu, D. Y. C. Leung, H. Wang, M. K. H. Leung and J. Xuan, *ChemElectroChem*, 2014, **1**, 836–849.
5 D. Sun, X. Xu, Y. Qin, S. P. Jiang and Z. Shao, *ChemSusChem*, 2020, **13**, 39–58.
6 A. Bagger, W. Ju, A. S. Varela, P. Strasser and J. Rossmeisl, *ChemPhysChem*, 2017, **18**, 3266–3273.
7 J. T. Feaster, C. Shi, E. R. Cave, T. Hatsukade, D. N. Abram, K. P. Kuhl, C. Hahn, J. K. Nørskov and T. F. Jaramillo, *ACS Catal.*, 2017, **7**, 4822–4827.
8 A. Wuttig, M. Yaguchi, K. Motobayashi, M. Osawa and Y. Surendranath, *Proc. Natl. Acad. Sci. U.S.A.*, 2016, **113**, E4585.
9 R. Kortlever, J. Shen, K. J. P. Schouten, F. Calle-Vallejo and M. T. M. Koper, *J. Phys. Chem. Lett.*, 2015, **6**, 4073–4082.
10 K. J. P. Schouten, Z. Qin, E. Pérez Gallent and M. T. M. Koper, *J. Am. Chem. Soc.*, 2012, **134**, 9864–9867.
11 A. A. Peterson, F. Abild-Pedersen, F. Studt, J. Rossmeisl and J. K. Nørskov, *Energy Environ. Sci.*, 2010, **3**, 1311–1315.
12 J. H. Montoya, A. A. Peterson and J. K. Nørskov, *ChemCatChem*, 2013, **5**, 737–742.
13 F. Calle-Vallejo and M. T. M. Koper, *Angew. Chem. Int. Ed.*, 2013, **52**, 7282–7285.
14 H. Xiao, T. Cheng, W. A. Goddard and R. Sundararaman, *J. Am. Chem. Soc.*, 2016, **138**, 483–486.
15 K. P. Kuhl, E. R. Cave, D. N. Abram and T. F. Jaramillo, *Energy Environ. Sci.*, 2012, **5**, 7050–7059.
16 S. Nitopi, E. Bertheussen, S. B. Scott, X. Liu, A. K. Engstfeld, S. Horch, B. Seger, I. E. L. Stephens, K. Chan, C. Hahn, J. K. Nørskov, T. F. Jaramillo and I. Chorkendorff, *Chem. Rev.*, 2019, **119**, 7610–7672.
17 D. Raciti and C. Wang, *ACS Energy Lett.*, 2018, **3**, 1545–1556.
18 G. F. Manbeck and E. Fujita, *J. Porphyr. Phthalocyanines*, 2015, **19**, 45–64.
19 J.-P. Jones, G. K. S. Prakash and G. A. Olah, *Isr. J. Chem.*, 2014, **54**, 1451–1466.
20 R. J. Lim, M. Xie, M. A. Sk, J.-M. Lee, A. Fisher, X. Wang and K. H. Lim, *Catal. Today*, 2014, **233**, 169–180.
21 K. Elouarzaki, V. Kannan, V. Jose, H. S. Sabharwal and J.-M. Lee, *Adv. Energy Mater.*, 2019, **9**, 1900090.
22 H. Fei, J. Dong, D. Chen, T. Hu, X. Duan, I. Shakir, Y. Huang and X. Duan, *Chem. Soc. Rev.*, 2019, **48**, 5207–5241.
23 M. Li, H. Wang, W. Luo, P. C. Sherrell, J. Chen and J. Yang, *Adv. Mater.*, 2020, **32**, 2001848.
24 A. S. Varela, W. Ju, A. Bagger, P. Franco, J. Rossmeisl and P. Strasser, *ACS Catal.*, 2019, **9**, 7270–7284.
25 E. González-Cervantes, A. A. Crisóstomo, A. Gutiérrez-Alejandre and A. S. Varela, *ChemCatChem*, 2019, **11**, 4854–4861.
26 T. Möller, W. Ju, A. Bagger, X. Wang, F. Luo, T. Ngo Thanh, A. S. Varela, J. Rossmeisl and P. Strasser, *Energy Environ. Sci.*, 2019, **12**, 640–647.
27 N. Leonard, W. Ju, I. Sinev, J. Steinberg, F. Luo, A. S. Varela, B. Roldan Cuenya and P. Strasser, *Chem. Sci.*, 2018, **9**, 5064–5073.
28 D. Yang and B. C. Gates, *ACS Catal.*, 2019, **9**, 1779–1798.
29 A. H. Chughtai, N. Ahmad, H. A. Younus, A. Laypkov and F. Verpoort, *Chem. Soc. Rev.*, 2015, **44**, 6804–6849.
30 P.-Q. Liao, J.-Q. Shen and J.-P. Zhang, *Coord. Chem. Rev.*, 2018, **373**, 22–48.
31 A. M. Szczepkowska, M. Janeta, M. Siczek, W. Tylus, A. M. Trzeciak and W. Bury, *Dalton Trans.*, 2021, **50**, 9051–9058.
32 G. R. Lorzing, K. P. Balto, A. M. Antonio, B. A. Trump, C. M. Brown and E. D. Bloch, *Chem. Mater.*, 2020, **32**, 7710–7715.
33 W. Morris, C. J. Stevens, R. E. Taylor, C. Dybowski, O. M. Yaghi and M. A. Garcia-Garibay, *J. Phys. Chem. C*, 2012, **116**, 13307–13312.
34 J. Duan, S. Chen and C. Zhao, *Nat. Commun.*, 2017, **8**, 15341.
35 W. Cheng, X. Zhao, H. Su, F. Tang, W. Che, H. Zhang and Q. Liu, *Nat. Energy*, 2019, **4**, 115–122.
36 M. Jahan, Q. Bao and K. P. Loh, *J. Am. Chem. Soc.*, 2012, **134**, 6707–6713.
37 X.-H. Liu, W.-L. Hu, W.-J. Jiang, Y.-W. Yang, S. Niu, B. Sun, J. Wu and J.-S. Hu, *ACS Appl. Mater. Interfaces*, 2017, **9**, 28473–28477.
38 R. Senthil Kumar, S. Senthil Kumar and M. Anbu Kulandainathan, *Electrochem. Commun.*, 2012, **25**, 70–73.
39 Y.-R. Wang, Q. Huang, C.-T. He, Y. Chen, J. Liu, F.-C. Shen and Y.-Q. Lan, *Nat. Commun.*, 2018, **9**, 4466.
40 S. Kempahanumakkagari, K. Vellingiri, A. Deep, E. E. Kwon, N. Bolan and K.-H. Kim, *Coord. Chem. Rev.*, 2018, **357**, 105–129.
41 S. R. Ahrenholtz, C. C. Epley and A. J. Morris, *J. Am. Chem. Soc.*, 2014, **136**, 2464–2472.
42 B. A. Johnson, A. M. Beiler, B. D. McCarthy and S. Ott, *J. Am. Chem. Soc.*, 2020, **142**, 11941–11956.
43 S. Goswami, I. Hod, J. D. Duan, C.-W. Kung, M. Rimoldi, C. D. Malliakas, R. H. Palmer, O. K. Farha and J. T. Hupp, *J. Am. Chem. Soc.*, 2019, **141**, 17696–17702.
44 P. J. Celis-Salazar, M. Cai, C. A. Cucinell, S. R. Ahrenholtz, C. C. Epley, P. M. Usov and A. J. Morris, *J. Am. Chem. Soc.*, 2019, **141**, 11947–11953.
45 P. A. Herrera-Herrera, E. Rodríguez-Sevilla and A. S. Varela, *Dalton Trans.*, 2021, **50**, 16939–16944.
46 M. Cai, Q. Loague and A. J. Morris, *J. Phys. Chem. Lett.*, 2020, **11**, 702–709.
47 P. Li and B. Wang, *Isr. J. Chem.*, 2018, **58**, 1010–1018.
48 L. S. Xie, G. Skorupskii and M. Dincă, *Chem. Rev.*, 2020, **120**, 8536–8580.
49 C.-W. Kung, K. Otake, C. T. Buru, S. Goswami, Y. Cui, J. T. Hupp, A. M. Spokoyny and O. K. Farha, *J. Am. Chem. Soc.*, 2018, **140**, 3871–3875.
50 Z. Xin, Y.-R. Wang, Y. Chen, W.-L. Li, L.-Z. Dong and Y.-Q. Lan, *Nano Energy*, 2020, **67**, 104233.
51 L. Sun, T. Miyakai, S. Seki and M. Dincă, *J. Am. Chem. Soc.*, 2013, **135**, 8185–8188.
52 D. Sheberla, L. Sun, M. A. Blood-Forsythe, S. Er, C. R. Wade, C. K. Brozek, A. Aspuru-Guzik and M. Dincă, *J. Am. Chem. Soc.*, 2014, **136**, 8859–8862.
53 A. J. Clough, J. M. Skelton, C. A. Downes, A. A. de la Rosa, J. W. Yoo, A. Walsh, B. C. Melot and S. C. Marinescu, *J. Am. Chem. Soc.*, 2017, **139**, 10863–10867.

54 D. Feng, T. Lei, M. R. Lukatskaya, J. Park, Z. Huang, M. Lee, L. Shaw, S. Chen, A. A. Yakovenko, A. Kulkarni, J. Xiao, K. Fredrickson, J. B. Tok, X. Zou, Y. Cui and Z. Bao, *Nat. Energy*, 2018, **3**, 30–36.
55 L. S. Xie, E. V. Alexandrov, G. Skorupskii, D. M. Proserpio and M. Dincă, *Chem. Sci.*, 2019, **10**, 8558–8565.
56 S. S. Park, E. R. Hontz, L. Sun, C. H. Hendon, A. Walsh, T. Van Voorhis and M. Dincă, *J. Am. Chem. Soc.*, 2015, **137**, 1774–1777.
57 S. Chen, J. Dai and X. C. Zeng, *Phys. Chem. Chem. Phys.*, 2015, **17**, 5954–5958.
58 M. E. Foster, K. Sohlberg, C. D. Spataru and M. D. Allendorf, *J. Phys. Chem. C*, 2016, **120**, 15001–15008.
59 T. Chen, J.-H. Dou, L. Yang, C. Sun, N. J. Libretto, G. Skorupskii, J. T. Miller and M. Dincă, *J. Am. Chem. Soc.*, 2020, **142**, 12367–12373.
60 E. M. Miner, T. Fukushima, D. Sheberla, L. Sun, Y. Surendranath and M. Dincă, *Nat. Commun.*, 2016, **7**, 10942.
61 D. Xing, Y. Wang, P. Zhou, Y. Liu, Z. Wang, P. Wang, Z. Zheng, H. Cheng, Y. Dai and B. Huang, *Appl. Catal., B*, 2020, **278**, 119295.
62 H. Huang, Y. Zhao, Y. Bai, F. Li, Y. Zhang and Y. Chen, *Adv. Sci.*, 2020, **7**, 2000012.
63 J.-D. Yi, D.-H. Si, R. Xie, Q. Yin, M.-D. Zhang, Q. Wu, G.-L. Chai, Y.-B. Huang and R. Cao, *Angew. Chem. Int. Ed.*, 2021, **60**, 17108–17114.
64 Z. Meng, J. Luo, W. Li and K. A. Mirica, *J. Am. Chem. Soc.*, 2020, **142**, 21656–21669.
65 N. C. Burtch, H. Jasuja and K. S. Walton, *Chem. Rev.*, 2014, **114**, 10575–10612.
66 M. Ding, X. Cai and H.-L. Jiang, *Chem. Sci.*, 2019, **10**, 10209–10230.
67 J. Duan, W. Jin and S. Kitagawa, *Coord. Chem. Rev.*, 2017, **332**, 48–74.
68 S. Yuan, L. Feng, K. Wang, J. Pang, M. Bosch, C. Lollar, Y. Sun, J. Qin, X. Yang, P. Zhang, Q. Wang, L. Zou, Y. Zhang, L. Zhang, Y. Fang, J. Li and H.-C. Zhou, *Adv. Mater.*, 2018, **30**, 1704303.
69 M. Moura de Salles Pupo and R. Kortlever, *ChemPhysChem*, 2019, **20**, 2926–2935.
70 P. Anastas and N. Eghbali, *Chem. Soc. Rev.*, 2010, **39**, 301–312.
71 K. S. Park, Z. Ni, A. P. Côté, J. Y. Choi, R. Huang, F. J. Uribe-Romo, H. K. Chae, M. O'Keeffe and O. M. Yaghi, *Proc. Natl. Acad. Sci. U.S.A.*, 2006, **103**, 10186.
72 S. Dou, J. Song, S. Xi, Y. Du, J. Wang, Z.-F. Huang, Z. J. Xu and X. Wang, *Angew. Chem. Int. Ed.*, 2019, **58**, 4041–4045.
73 Y. Wang, P. Hou, Z. Wang and P. Kang, *ChemPhysChem*, 2017, **18**, 3142–3147.
74 J.-X. Wu, W.-W. Yuan, M. Xu and Z.-Y. Gu, *Chem. Commun.*, 2019, **55**, 11634–11637.
75 X. Jiang, H. Li, J. Xiao, D. Gao, R. Si, F. Yang, Y. Li, G. Wang and X. Bao, *Nano Energy*, 2018, **52**, 345–350.
76 B. D. McCarthy, A. M. Beiler, B. A. Johnson, T. Liseev, A. T. Castner and S. Ott, *Coord. Chem. Rev.*, 2020, **406**, 213137.
77 J. Huang, Y. Li, R.-K. Huang, C.-T. He, L. Gong, Q. Hu, L. Wang, Y.-T. Xu, X.-Y. Tian, S.-Y. Liu, Z.-M. Ye, F. Wang, D.-D. Zhou, W.-X. Zhang and J.-P. Zhang, *Angew. Chem. Int. Ed.*, 2018, **57**, 4632–4636.
78 K. Rui, G. Zhao, Y. Chen, Y. Lin, Q. Zhou, J. Chen, J. Zhu, W. Sun, W. Huang and S. X. Dou, *Adv. Funct. Mater.*, 2018, **28**, 1801554.
79 F. Yang, A. Chen, P. L. Deng, Y. Zhou, Z. Shahid, H. Liu and B. Y. Xia, *Chem. Sci.*, 2019, **10**, 7975–7981.
80 S. Zhao, C. Tan, C.-T. He, P. An, F. Xie, S. Jiang, Y. Zhu, K.-H. Wu, B. Zhang, H. Li, J. Zhang, Y. Chen, S. Liu, J. Dong and Z. Tang, *Nat. Energy*, 2020, **5**, 881–890.
81 L. Wang, Y. Wu, R. Cao, L. Ren, M. Chen, X. Feng, J. Zhou and B. Wang, *ACS Appl. Mater. Interfaces*, 2016, **8**, 16736–16743.
82 J.-X. Wu, S.-Z. Hou, X.-D. Zhang, M. Xu, H.-F. Yang, P.-S. Cao and Z.-Y. Gu, *Chem. Sci.*, 2019, **10**, 2199–2205.
83 M. Jiang, L. Li, D. Zhu, H. Zhang and X. Zhao, *J. Mater. Chem. A*, 2014, **2**, 5323–5329.
84 J. Albo, D. Vallejo, G. Beobide, O. Castillo, P. Castaño and A. Irabien, *ChemSusChem*, 2017, **10**, 1100–1109.
85 M. Perfecto-Irigaray, J. Albo, G. Beobide, O. Castillo, A. Irabien and S. Pérez-Yáñez, *RSC Adv.*, 2018, **8**, 21092–21099.
86 H. Sun, Z. Yan, F. Liu, W. Xu, F. Cheng and J. Chen, *Adv. Mater.*, 2020, **32**, 1806326.
87 H. Ji, S. Hwang, K. Kim, C. Kim and N. C. Jeong, *ACS Appl. Mater. Interfaces*, 2016, **8**, 32414–32420.
88 Z. Dou, J. Yu, H. Xu, Y. Cui, Y. Yang and G. Qian, *Thin Solid Films*, 2013, **544**, 296–300.
89 C.-P. Wang, H.-Y. Liu, G. Bian, X. Gao, S. Zhao, Y. Kang, J. Zhu and X.-H. Bu, *Small*, 2019, **15**, 1906086.
90 L. Yang, G. Zhu, H. Wen, X. Guan, X. Sun, H. Feng, W. Tian, D. Zheng, X. Cheng and Y. Yao, *J. Mater. Chem. A*, 2019, **7**, 8771–8776.
91 N. Kornienko, Y. Zhao, C. S. Kley, C. Zhu, D. Kim, S. Lin, C. J. Chang, O. M. Yaghi and P. Yang, *J. Am. Chem. Soc.*, 2015, **137**, 14129–14135.
92 D.-J. Li, Q.-H. Li, Z.-G. Gu and J. Zhang, *J. Mater. Chem. A*, 2019, **7**, 18519–18528.
93 L. Ye, J. Liu, Y. Gao, C. Gong, M. Addicoat, T. Heine, C. Wöll and L. Sun, *J. Mater. Chem. A*, 2016, **4**, 15320–15326.
94 H. K. Arslan, O. Shekhah, D. C. F. Wieland, M. Paulus, C. Sternemann, M. A. Schroer, S. Tiemeyer, M. Tolan, R. A. Fischer and C. Wöll, *J. Am. Chem. Soc.*, 2011, **133**, 8158–8161.
95 B. Liu and R. A. Fischer, *Sci. China: Chem.*, 2011, **54**, 1851–1866.
96 M. L. Ohnsorg, C. K. Beaudoin and M. E. Anderson, *Langmuir*, 2015, **31**, 6114–6121.
97 I. Hod, M. D. Sampson, P. Deria, C. P. Kubiak, O. K. Farha and J. T. Hupp, *ACS Catal.*, 2015, **5**, 6302–6309.
98 X. Kang, Q. Zhu, X. Sun, J. Hu, J. Zhang, Z. Liu and B. Han, *Chem. Sci.*, 2016, **7**, 266–273.
99 X. Kang, B. Wang, K. Hu, K. Lyu, X. Han, B. F. Spencer, M. D. Frogley, F. Tuna, E. J. L. McInnes, R. A. W. Dryfe,

B. Han, S. Yang and M. Schröder, *J. Am. Chem. Soc.*, 2020, **142**, 17384–17392.
100 R. Hinogami, S. Yotsuhashi, M. Deguchi, Y. Zenitani, H. Hashiba and Y. Yamada, *ECS Electrochem. Lett.*, 2012, **1**, H17–H19.
101 H. Zhang, J. Li, Q. Tan, L. Lu, Z. Wang and G. Wu, *Chem.–Eur. J.*, 2018, **24**, 18137–18157.
102 B.-X. Dong, S.-L. Qian, F.-Y. Bu, Y.-C. Wu, L.-G. Feng, Y.-L. Teng, W.-L. Liu and Z.-W. Li, *ACS Appl. Energy Mater.*, 2018, **1**, 4662–4669.
103 C. Costentin, S. Drouet, M. Robert and J.-M. Savéant, *Science*, 2012, **338**, 90–94.
104 I. Choi, Y. E. Jung, S. J. Yoo, J. Y. Kim, H.-J. Kim, C. Y. Lee and J. H. Jang, *J. Electrochem. Sci. Technol.*, 2017, **8**, 61–68.
105 F. Sun, G. Wang, Y. Ding, C. Wang, B. Yuan and Y. Lin, *Adv. Energy Mater.*, 2018, **8**, 1800584.
106 A. S. Varela, *Curr. Opin. Green Sustain. Chem.*, 2020, **26**, 100371.
107 M.-D. Zhang, D.-H. Si, J.-D. Yi, Q. Yin, Y.-B. Huang and R. Cao, *Sci. China: Chem.*, 2021, **64**, 1332–1339.
108 H. Zhong, M. Ghorbani-Asl, K. H. Ly, J. Zhang, J. Ge, M. Wang, Z. Liao, D. Makarov, E. Zschech, E. Brunner, I. M. Weidinger, J. Zhang, A. V. Krasheninnikov, S. Kaskel, R. Dong and X. Feng, *Nat. Commun.*, 2020, **11**, 1409.
109 R. Matheu, E. Gutierrez-Puebla, M. Á. Monge, C. S. Diercks, J. Kang, M. S. Prévot, X. Pei, N. Hanikel, B. Zhang, P. Yang and O. M. Yaghi, *J. Am. Chem. Soc.*, 2019, **141**, 17081–17085.
110 L. Majidi, A. Ahmadiparidari, N. Shan, S. N. Misal, K. Kumar, Z. Huang, S. Rastegar, Z. Hemmat, X. Zou, P. Zapol, J. Cabana, L. A. Curtiss and A. Salehi-Khojin, *Adv. Mater.*, 2021, **33**, 2004393.
111 J. Li, P. Pršlja, T. Shinagawa, A. J. Martín Fernández, F. Krumeich, K. Artyushkova, P. Atanassov, A. Zitolo, Y. Zhou, R. García-Muelas, N. López, J. Pérez-Ramírez and F. Jaouen, *ACS Catal.*, 2019, **9**, 10426–10439.
112 W. Ju, A. Bagger, G.-P. Hao, A. S. Varela, I. Sinev, V. Bon, B. Roldan Cuenya, S. Kaskel, J. Rossmeisl and P. Strasser, *Nat. Commun.*, 2017, **8**, 944.
113 G. Xing, L. Cheng, K. Li, Y. Gao, H. Tang, Y. Wang and Z. Wu, *Appl. Surf. Sci.*, 2021, **550**, 149389.
114 Y. Tian, Y. Wang, L. Yan, J. Zhao and Z. Su, *Appl. Surf. Sci.*, 2019, **467–468**, 98–103.
115 T. Bligaard and J. K. Nørskov, *Electrochim. Acta*, 2007, **52**, 5512–5516.
116 X. Mao, C. Tang, T. He, D. Wijethunge, C. Yan, Z. Zhu and A. Du, *Nanoscale*, 2020, **12**, 6188–6194.
117 D. Choukroun, N. Daems, T. Kenis, T. Van Everbroeck, J. Hereijgers, T. Altantzis, S. Bals, P. Cool and T. Breugelmans, *J. Phys. Chem. C*, 2020, **124**, 1369–1381.
118 W. Zhou, D.-D. Huang, Y.-P. Wu, J. Zhao, T. Wu, J. Zhang, D.-S. Li, C. Sun, P. Feng and X. Bu, *Angew. Chem. Int. Ed.*, 2019, **58**, 4227–4231.
119 X.-L. Wang, L.-Z. Dong, M. Qiao, Y.-J. Tang, J. Liu, Y. Li, S.-L. Li, J.-X. Su and Y.-Q. Lan, *Angew. Chem. Int. Ed.*, 2018, **57**, 9660–9664.
120 W. Ren, X. Tan, W. Yang, C. Jia, S. Xu, K. Wang, S. C. Smith and C. Zhao, *Angew. Chem. Int. Ed.*, 2019, **58**, 6972–6976.
121 H. Yuan and Z. Li, *J. Phys. Chem. C*, 2021, **125**, 18180–18186.
122 Z. Xue, Y. Li, Y. Zhang, W. Geng, B. Jia, J. Tang, S. Bao, H.-P. Wang, Y. Fan, Z.-w. Wei, Z. Zhang, Z. Ke, G. Li and C.-Y. Su, *Adv. Energy Mater.*, 2018, **8**, 1801564.